Graphical Abstract

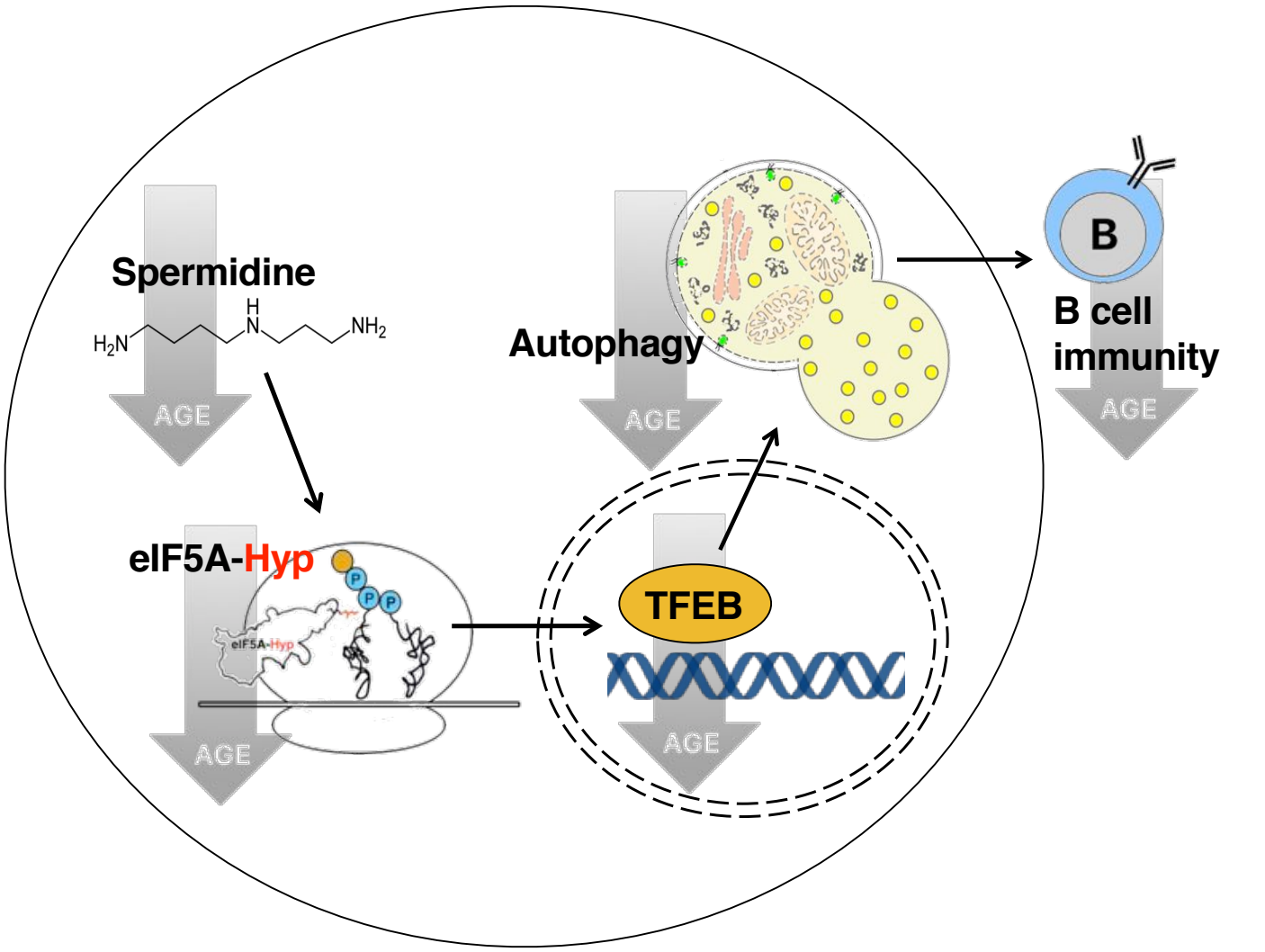

Translational control of TFEB and autophagy via eIF5A rejuvenates B cell immunity

Hanlin Zhang[1], Ghada Alsaleh[1^], Jack Feltham[2^], Yizhe Sun[1], Thomas Riffelmacher[1], Philip Charles[2,3], Lisa Frau[1], Zhanru Yu[3], Shabaz Mohammed[2], Stefan Balabanov[4], Jane Mellor[2], Anna Katharina Simon[1*]

[1]*The Kennedy Institute of Rheumatology, University of Oxford, Roosevelt Drive, Oxford OX3 7FY, UK*

[2]*Department of Biochemistry, University of Oxford, South Parks Road, Oxford OX1 3Q, UK*

[3]*Target Discovery Institute, University of Oxford, Roosevelt Drive, Oxford OX3 7FZ, UK*

[4]*Division of Haematology, University Hospital and University of Zürich, 8091 Zürich, Switzerland*

^ *equal contribution*

* *Corresponding author, The Kennedy Institute of Rheumatology, University of Oxford, Roosevelt Drive, Oxford OX3 7FY, UK*

Abstract

Failure to make adaptive immune responses is a hallmark of aging. In particular reduced B cell function leads to poor vaccination efficacy and a high prevalence of infections in the elderly. However, the molecular mechanism underlying immune senescence is largely unknown. Here we show that autophagy levels are specifically reduced in mature lymphoid cells, leading to compromised memory B cell responses in old individuals. Mechanistically, the polyamine metabolite spermidine post-translationally modifies the translation factor eIF5A, which assists the synthesis of TFEB, a key transcription factor of autophagy. Spermidine is depleted in the elderly, leading to reduced TFEB expression and autophagy. Replenishing spermidine restored this pathway and improved the responses of both old mouse and old human B cells. Taken together, our results reveal a novel autophagy regulatory mechanism mediated by eIF5A at the translational level, and this pathway can be harnessed to rejuvenate immune senescence in humans.

Immune senescence is characterized by the failure of lymphocytes to respond adequately to infection, malignancy, and vaccination. Infectious diseases are still the fourth most common cause of death among the elderly in the developed world. During a regular influenza season, about 90% of the excess deaths occur in people aged over 65[1]. Immune responses to vaccines are known to be particular ineffective in the elderly population (>65yrs), and yet some vaccines, such as influenza, are primarily given to the elderly. A major correlate of protection for vaccinations is the specific antibody titer generated by long-lived plasma B cells. With a life span of up to several decades, long-lived lymphocytes are particularly prone to accumulate waste over time. Autophagy recycles unwanted cytoplasmic material. Lymphocytes deficient in autophagy are unable to generate adequate responses, in particular long-lived lymphocytes, i.e. memory T and B cells or plasma B cells[2-5]. Reversing or halting immune ageing would open opportunities to improve management of age-related morbidities and have a major impact on the health status of society. However, little is known about how immune senescence can be reversed.

Genetic activation of autophagy extends lifespan in mice[6, 7]. However, only a handful of autophagy-inducing drugs have been shown to reverse aging, one being rapamycin, an inhibitor of mTOR[8]. Due to the unwanted effects of mTOR inhibition, there is a need to better understand mTOR-independent control of autophagy for drug development. Furthermore, to test anti-aging drugs, biomarkers that can be measured in blood are critical. Previously we found that spermidine reverses aging of the memory T cell response[3] and Eisenberg *et al*.

rejuvenated cardiac function with spermidine[9], both in mice, in an autophagy-dependent manner. As an endogenous polyamine metabolite that declines with age, spermidine may be key in controlling cellular aging via autophagy. However the target of spermidine and the mechanism by which it regulates autophagy is still controversial. Here we investigated whether spermidine is able to rejuvenate long-term B cell responses, the main correlate of protection for vaccination. We found an autophagy-dependent improvement of old B cell responses by spermidine, indicating that it has rejuvenating effects across different immune cell types. Using ribosome profiling, proteomics and biochemical assays, we show that the post-translational modification (hypusination) of eIF5A by spermidine regulates both protein synthesis and autophagy in primary B cells. Due to the rigid structure of proline, triprolines slow down translation and require hypusinated eIF5A to form peptide bonds more effectively[10]. We find this is specifically required for the translation of the autophagosomal/lysosomal master regulator TFEB[11], which contains one triproline motif in mouse and two in human. Moreover, in human B cells spermidine improves hypusination of eIF5A, TFEB protein expression, autophagic flux and antibody titers, which has direct translational relevance. Lastly this pathway is considerably downregulated in the elderly, making its components suitable biomarkers.

Spermidine rejuvenates B cell responses in old mice via induction of autophagy.

We have demonstrated that autophagic flux is decreased with age in human and murine T cells[3, 12]. Here we first investigated the extent of the decrease across bone marrow progenitors and mature hematopoietic cells including B cells, with a novel method of quantifying endogenous LC3-II, a marker for autophagosomes, by flow cytometry. To measure active autophagic flux, bafilomycin A1 (BafA1) was used which is a lysosomal V-ATPase inhibitor that prevents acidification of lysosomes and their degradative functions, thereby causing accumulation of autophagic substrates including LC3-II. Autophagic flux was mildly reduced in hematopoietic stem cells (HSCs), and most significantly in B and T cells from old mice as compared to young mice (Fig. 1a/g, gating strategy in S1a and 1b). Treatment of mice for 6 weeks with spermidine increased autophagic flux in these hematopoietic cell types (Fig. 1a and 1b). This was confirmed in B lymphocytes by Western blot (Fig. 1c) and by confocal microscopy using GFP-LC3 transgenic mice (Fig. 1d). Old B lymphocytes accumulated LC3-II, which did not further increase by BafA1 treatment (Fig. 1c and 1d). This indicates that autophagic flux is impaired in old cells at the level of the lysosome. We then tested if the *in vivo* administration of spermidine alleviates typical hallmarks of hematopoietic aging[13] such as expanded HSCs and $Lin^{-}Sca1^{+}cKit^{+}$ cells (LSKs) (Fig. S1a for gating and S1c), myeloproliferation and lymphopenia (Fig. S1b for gating, S1d-1f). However, spermidine does

Figure 1 Spermidine rejuvenates B cell responses in old mice via induction of autophagy.

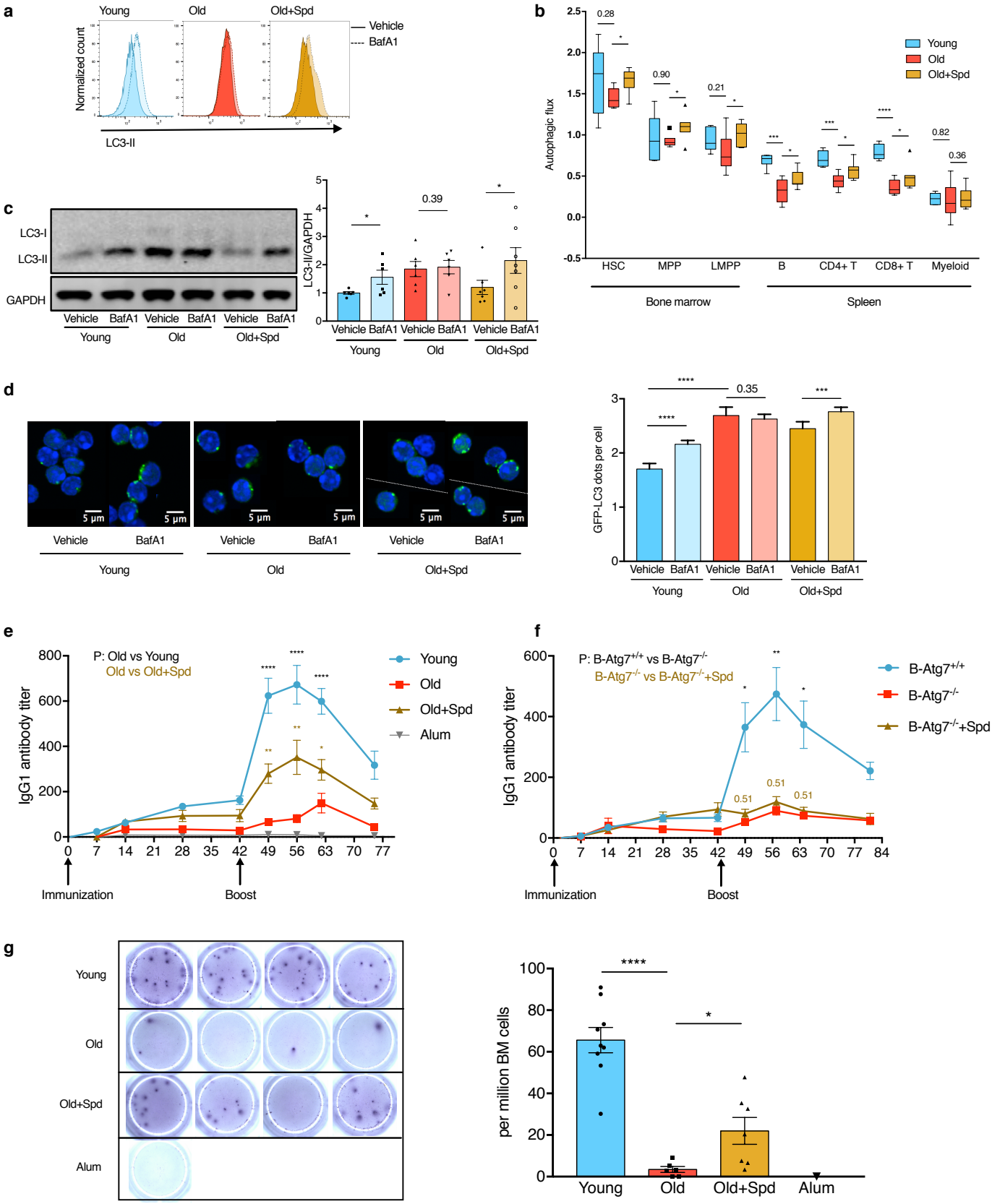

Figure 1. Spermidine rejuvenates B cell responses in old mice via induction of autophagy.

(a/b) The autophagic flux of B cells (a, representative plots) and other indicated cell types (b, quantification) from young (12 weeks) and old (22-24 months) mice, and old mice administered with spermidine for 6 weeks was measured by LC3-II staining using flow cytometry after 2 h treatment with 10 nM bafilomycin A1 (BafA1) or vehicle. (See Fig. S1a and S1b for gating strategy). Autophagic flux was calculated as LC3-II geometric mean fluorescence intensity (BafA1-Vehicle)/Vehicle. n = 5/6/7 mice for Young/Old/Old+Spd respectively. Two-tailed Student's t-test for Young/Old comparison, one-tailed Student's t-test for Old/Old+Spd comparison. See Fig. S1 c-i for spermidine's effect on aged haematopoiesis.

(c) LC3-II of purified B cells from wild type mice (treated as in a) was assessed by Western blot. The densitometric quantification is shown in the right panel. n = 6-7 mice as indicated by dots. Paired one-tailed Student's t-test.

(d) Representative confocal microscopy images of purified B cells from GFP-LC3 transgenic mice. The quantification of GFP-LC3 dots per cell is shown in the right panel. N = 210-616 cells from 4-6 mice, Mann-Whitney test.

(e) Young or old mice were immunized and boosted with NP-CGG. Spermidine was given 2 days before the first immunization and then continuously in drinking water. Serum NP-specific IgG1 titers were measured by ELISA. n = 14 (Young) or 10 (Old/Old+Spd) mice from 2 experiments.

(f) B cell-specific *Atg7* knockout mice (*Mb1-Cre*, $Atg7^{f/f}$) (Fig. S1j and S1k) were immunized and IgG1 responses assessed as in E. n = 7 (B-$Atg7^{+/+}$) or 3 (B-$Atg7^{-/-}$) mice.

(g) Mice from E were culled on day 75 and long-lived bone marrow plasma cells secreting NP-specific IgG1 were measured by ELISpot. Representative images (left) and the quantification (right) are shown. n = 6-9 mice as indicated by dots.

Welch's t-test for e/f/g. P values were adjusted by the Holm-Sidak method for multiple comparisons of the three time points in e/f.

Data represented as box-and-whisker plots showing whiskers and outliers by Tukey method (b) or as mean ± SEM (c-g). *P≤0.05, **P≤0.01, ***P≤0.001, ****P≤0.0001.

not affect the typical signs of hematopoietic aging (Fig. S1c and S1f). Nor does it have any significant effect on B cell progenitor numbers in old bone marrow (Fig. S1g-i), or on lymphopenia and myeloid expansion typically found in old spleens (Fig. S1d).

We then examined whether spermidine improves B cell function. In mice over 22 months of age, the antibody response to immunization with the model antigen NP-CGG was markedly reduced as expected, but administration of spermidine in drinking water significantly improved IgG1 responses (Fig. 1e) in an autophagy-dependent manner using B-cell specific conditional deletion of *Atg7* (Fig. 1f, S1j and S1k for control for efficient deletion of *Atg7* and autophagy in B cells). At the time of sacrifice, we found very low numbers of long-lived bone marrow NP-specific plasma cells in old mice, which were significantly restored with spermidine treatment (Fig. 1g). This effect was not observed in young mice (Fig. S1l). Thus, spermidine restored autophagic flux in old B lymphocytes *in vivo* and rejuvenated B-cell responses in an autophagy-dependent manner, but did not reverse aging of hematopoietic stem and progenitor cells.

Spermidine maintains cellular autophagy by hypusinating eIF5A.

We next investigated how spermidine regulates autophagy. First, we confirmed 100 μM spermidine to be the optimal concentration to induce autophagy *in vitro* (Fig. S2a/b)[14, 15]. Several signaling pathways have been described downstream of spermidine, including inhibition of histone acetyltransferases (HATs)[16]. Therefore, we investigated whether spermidine inhibits HAT activity and thereby induces *Atg7* mRNA as shown in yeast[14]. In neither of three approaches (HAT colorimetric assay, acetylated H3 pull down, and *Atg7* qPCR) using the mammalian lymphocytic Jurkat cell line did we find that spermidine had this effect (Fig. S2c-2e). HATs have been shown to also directly acetylate certain autophagy proteins such as ATG7 to regulate autophagy[17]. However, ATG7 acetylation was not affected by two tested concentrations of spermidine over 6 hours (Fig. S2e and S2f). Spermidine also failed to affect the activity of AMPK as assessed by AMPK phosphorylation (Fig. S2g). However, we found that a dose of 100 μM or higher of spermidine induces ER stress (Fig. S2h), demonstrated by increased levels of ATF4 (Fig. S2i), phosphorylated eIF2α (Fig. S2j), and increased expression of *CHOP* mRNA (Fig. S2k). Furthermore, high-dose spermidine induced cell death after 24 h (Fig. S2l/m), presumably because spermidine levels are high in transformed cell lines and further uptake is toxic and non-specifically induces cellular stress responses, likely also inducing autophagy. In subsequent experiments, we opted for the depletion of spermidine either by genetic knock down of the key spermidine synthesizing enzyme ornithine decarboxylase (ODC), or the ODC inhibitor difluoromethylornithine (DFMO) (Fig. 2a). Indeed, genetic knock down of *Odc* with siRNA, or DFMO treatment,

reduces spermidine levels substantially, whilst supplementing cells with spermidine rescues its levels partially, as measured by GC-MS in cell lysates (Fig. 2b and S3a/b). This demonstrates firstly that cultured cells actively synthesize spermidine via ODC, and secondly that exogenous spermidine is efficiently taken up to rescue its intracellular levels.

Next, we examined pathways downstream of spermidine that had not been previously linked to autophagy. In eukaryotic cells spermidine is a unique substrate for the hypusination of the translation factor eIF5A (Fig. 2a)[18]. To date, eIF5A is the only known protein containing the unusual amino acid hypusine[10]. Upon knockdown of *Odc* in NIH 3T3 cells, or addition of the ODC inhibitor DFMO, we found reduced hypusinated eIF5A and LC3-II levels, while supplementation with spermidine rescues both (Fig. 2c and S3c-3e). Similarly, reduced LC3-II levels were observed when *Eif5a was* knocked down (Fig. 2d, S2f and S2g). We next depleted the two hypusinating enzymes deoxyhypusine synthase (DHS) and deoxyhypusine hydroxylase (DOHH) to study their effect on autophagy. The knockdown of *Dhs* or knockout of *Dohh* reduced eIF5A hypusination and LC3-II levels (Fig. 2e, and S3h-3j). Whilst exogenous spermidine restored LC3-II levels in cells depleted of spermidine, inhibition of eIF5A hypusination with *siDhs* or GC7, a specific inhibitor of DHS, abrogated this effect (Fig. 2f, S3k and S3l). Taken together these data indicate that hypusinated eIF5A regulates autophagy, and that spermidine maintains cellular autophagy by hypusinating eIF5A.

In activated T cells, eIF5A is one of the twenty most abundant proteins[19]. However, little is known about its role in lymphocytes. We measured eIF5A levels and autophagy in primary B cells during activation. LC3-II levels increased substantially over time upon activation in B cells, as measured by flow cytometry (Fig. 2g, quantified in Fig. S3m) and Western blot (Fig. 2h and S3n). This time-dependent increase correlated with increasing levels of both total and hypusinated eIF5A (Fig. 2h, S3n and S3o). In line with our data in cell lines, LC3-II levels decreased with increasing doses of GC7 (Fig. 2i and S3p). This pathway operates independently of mTOR whose activation inhibits autophagy. Indeed GC7 did not activate mTOR as demonstrated by S6 phosphorylation, a downstream substrate of mTOR (Fig. S3q). Overall this data indicates that the eIF5A-autophagy pathway is induced upon activation of primary B cells, and physiological levels of hypusinated eIF5A are required for efficient autophagy.

eIF5A hypusination is required for TFEB expression.

We next addressed how eIF5A regulates autophagy by identifying changes in expression of proteins involved in the autophagy pathway upon inhibition of eIF5A. For this we performed label-free quantitative mass spectrometry on nuclear and cytoplasmic fractions of activated

Figure 2 Spermidine maintains cellular autophagy by hypusinating eIF5A.

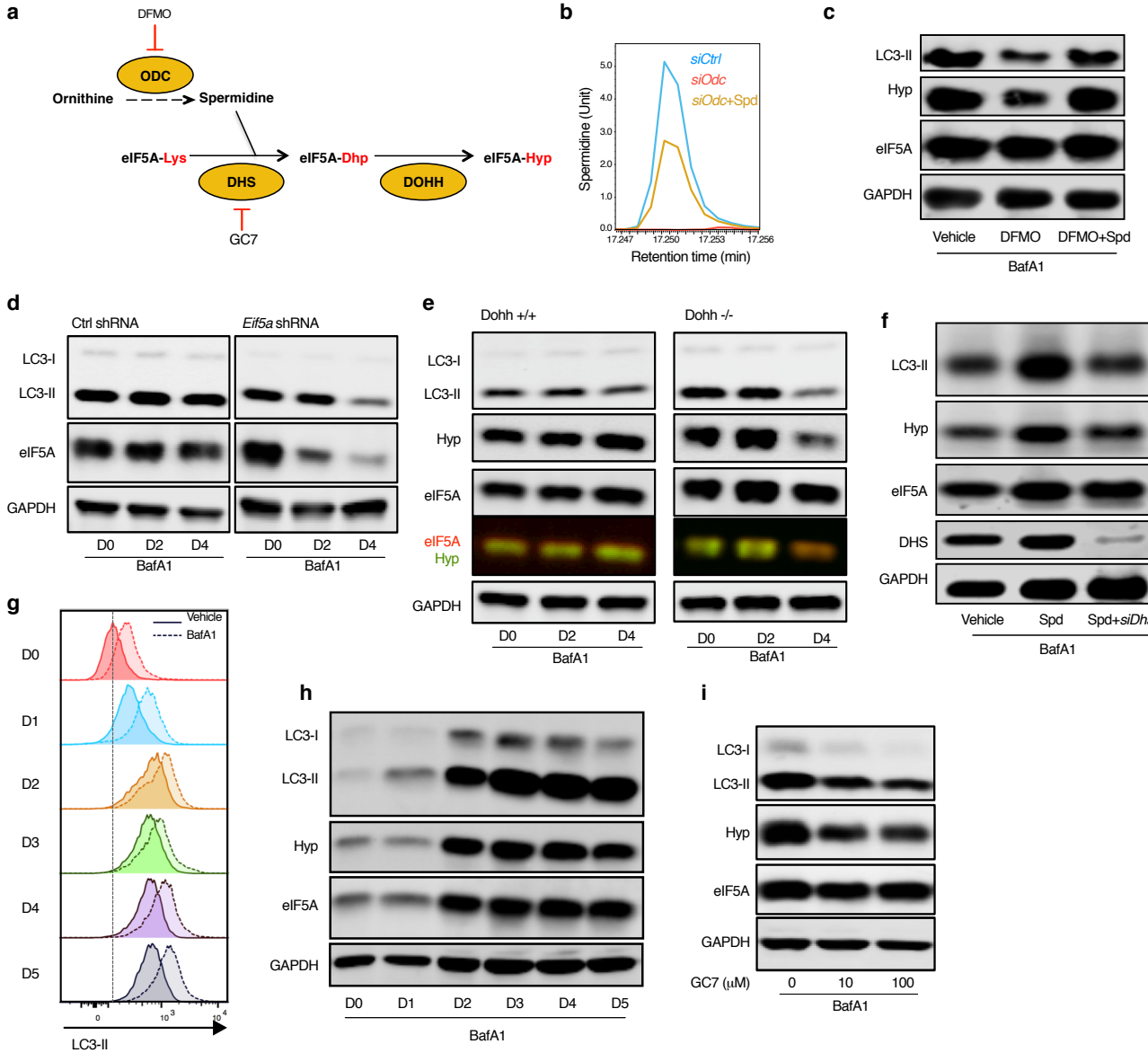

Figure 2. Spermidine maintains cellular autophagy by hypusinating eIF5A.

(a) Spermidine synthesis and eIF5A hypusination pathway in eukaryotes. Difluoromethylornithine (DFMO) is an irreversible inhibitor of the key spermidine synthesis enzyme ornithine decarboxylase (ODC). N1-Guanyl-1,7-Diaminoheptane (GC7) is a competitive inhibitor of the key hypusination enzyme deoxyhypusine synthase (DHS).

(b) NIH 3T3 cells were transfected with non-targeted siRNA (*siCtrl*), siRNA targeting *Odc* mRNA (*siOdc*) (Fig. S3a) and treated with 10 μM spermidine for 3 days where indicated. Cellular spermidine levels were determined by gas chromatography-mass spectrometry (GC-MS). Representative of 3 repeats. See Fig. S3b for quantifications.

(c) NIH 3T3 cells were treated with DFMO together with or without 10 uM spermidine for 24 h. Autophagy (LC3-II) and eIF5A hypusination (Hyp) were measured by Western blot. Representative of 3 repeats. LC3-II quantified in Fig. S3e. See also Fig. S3c-e.

(d) The knockdown of *Eif5a* was induced by 100 μM IPTG in NIH 3T3 cells expressing IPTG-inducible *Eif5a* shRNA. The expression of eIF5A and LC3-II on indicated days post IPTG induction was measured by Western blot. Representative of 3 repeats. Quantified in Fig. S3f. See also Fig. S3g.

(e) The knockout of *Dohh* was induced by 100 nM 4-OHT in immortalized transgenic mouse embryonic fibroblasts (Pallmann et al., 2015). eIF5A hypusination and LC3-II on indicated days post induction were measured by Western blot. Representative of 3 repeats. Quantified in Fig. S3i. See also Fig. S3h.

(f) Spermidine-depleted NIH 3T3 cells by *siOdc* transfection were rescued with spermidine alone or spermidine together with siRNA targeting *Dhs* mRNA (*siDhs*). eIF5A hypusination and LC3-II were measured 3 days post transfection by Western blot. Representative of 3 repeats. LC3-II quantified in Fig. S3k. See also Fig. S3j-l.

(g/h) B cells purified from young adult wild type mice were cultured with 10 μg/mL LPS for indicated days and LC3-II was measured by flow cytometry (g, quantified in Fig. S3m) and Western blot (h). The expression of overall eIF5A and its hypusination were assessed by Western blot (h, representative of 7 repeats, quantified in Fig. S3o). See also Fig. S3n.

(i) B cells were LPS-activated as in G and cultured for 3 days with indicated concentrations of GC7 added on day 2 for 24 h. eIF5A hypusination and LC3-II were measured by Western blot. Representative of 6 repeats. Quantified in Fig. S3p.

To measure autophagy, all cells were treated with 10 nM BafA1 for 2 h before harvesting.

primary B cells treated with GC7 (Fig. 3a and S4a). This was followed by stable isotope labeling with amino acids in cell culture (SILAC) on activated primary B cells (Fig. 3b and S4b). Of the autophagy related proteins detected, TFEB was the only protein repeatedly found decreased upon GC7 treatment in both approaches. TFEB is a key transcription factor regulating autophagosomal and lysosomal biogenesis[11, 20]. The effect of inhibition of eIF5A hypusination by GC7 on TFEB was confirmed by Western blot in activated primary B cells (Fig. 3c). Moreover, cellular fractionation demonstrated that TFEB protein is also decreased in the nuclear fraction (Fig. 3d). Accordingly, gene expression of several TFEB targets was markedly decreased in activated B cells upon GC7 treatment (Fig. 3e). Genetic knockdown of *Eif5a* and *Dhs* in NIH 3T3 cells similarly led to a decrease in TFEB protein (Fig. 3f, Fig. S4c and S4d). To test if TFEB is affected by spermidine depletion, we inhibited spermidine synthesis in NIH 3T3 cells by *siODC* or DFMO. This caused a reduction in TFEB, which was rescued by exogenous spermidine administration (Fig. 3g, Fig. S4e and S4f), suggesting that spermidine controls cellular TFEB levels. However, spermidine failed to maintain TFEB levels when *Eif5a* was knocked down or eIF5A hypusination was inhibited (Fig. 3h, S4g and S4h), indicating that the regulation of TFEB levels by spermidine is mediated via eIF5A hypusination.

Hypusinated eIF5A assists polyproline synthesis in B cells.

TFEB is a very short-lived protein (< 4 hours half-life)[21] compared to other proteins in the cell (median 36 hours half-life)[22], and is therefore expected to require more active translation than most proteins. We first investigated if eIF5A controls overall protein synthesis in lymphocytes as previously reported[23]. We measured translation by flow cytometry and found that depletion of spermidine by DFMO caused a reduction in protein synthesis rate, which was rescued by exogenous spermidine supply (Fig. S5a). Consistently, inhibition of eIF5A hypusination by GC7 also caused a time-dependent decrease of general protein synthesis (Fig. 4a).

Protein levels reflect the balance between protein synthesis and degradation. We therefore measured protein synthesis regulated by eIF5A hypusination alone using ribosome profiling in activated primary B cells, the first study of this kind in mammalian cells[24, 25]. Moreover, this technique, which measures ribosome occupancy at single nucleotide resolution, enabled us to investigate the regulation of synthesis of certain peptide sequences by hypusinated eIF5A. We found that eIF5A controls global translation at both initiation and termination (Fig. 4b and 4c). As observed in yeast and bacteria[24, 26, 27], a mild stalling of ribosomes at the triproline motif (PPP) was found in primary B cells, which was increased by GC7 treatment (Fig. 4d), indicating that solving the translational stalling at the polyproline motif is a

Figure 3 eIF5A hypusination is required for TFEB expression.

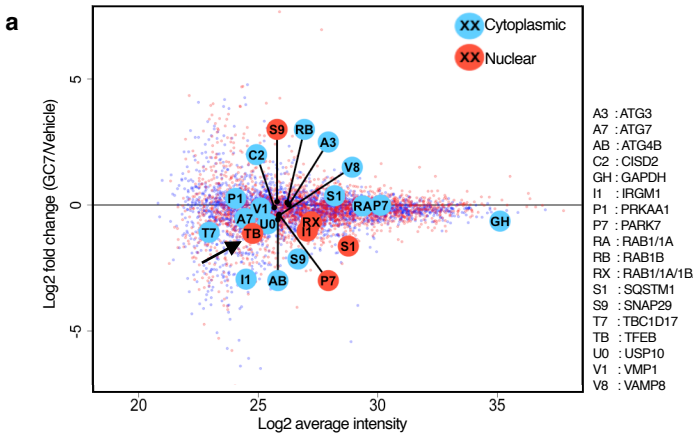

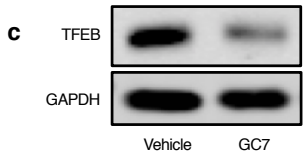

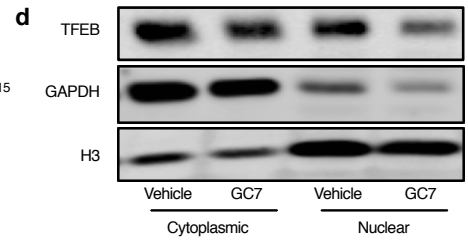

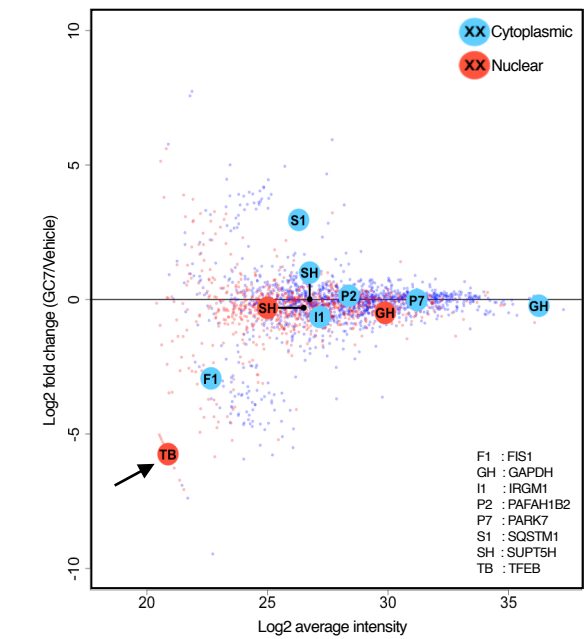

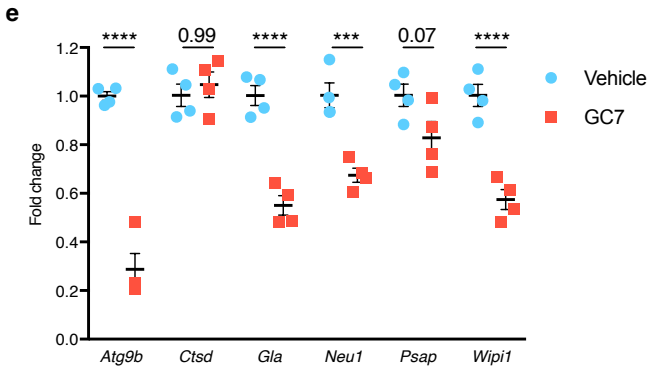

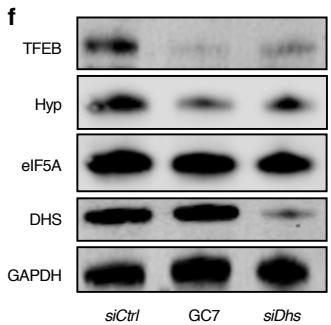

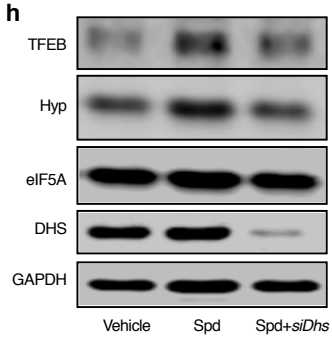

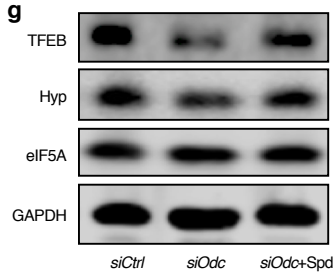

Figure 3. eIF5A hypusination is required for TFEB expression.

(a) Murine B cells were treated with 10 μM GC7 for 24 h as in Fig. 2i and fractionated for label-free quantitative protein mass spectrometry (MS) analysis (cell fractionation control in Fig. S4a). Identified autophagy proteins are highlighted by enlarged, annotated circles, and TFEB is further indicated by a black arrow.

(b) Murine B cells were cultured in medium containing amino acids with heavy isotope labeling (GC7-treated) or light isotopes (Vehicle). Cells that had divided four times were sorted by flow cytometry (Fig. S4b) and mixed at 1:1 ratio (heavy: light isotope labelling), followed by cell fractionation and protein MS analysis. For the repeat the labeling was swapped. Data represent the average of protein changes from the two repeats. Identified autophagy proteins are highlighted

(c-e) Murine B cells were treated with GC7 as in A. The overall TFEB (c), and cytoplasmic/nuclear TFEB (d) were assessed by Western blot. Representative of 3 independent repeats. (e) The expression of TFEB-target genes was measured by qPCR with *Gapdh* as reference gene. n = 4 mice. Two-way ANOVA with post hoc Sidak's test, ***P≤0.001, ****P≤0.0001. Data represented as mean ± SEM.

(f) NIH 3T3 cells were transfected with *siDhs* for 3 days or treated with 10 μM GC7 for 24 h. TFEB expression was measured by Western blot. Representative of 3 repeats. Quantified in Fig. S4c. See also Fig. S4d.

(g) NIH 3T3 cells were transfected with *siOdc* with or without 10 μM spermidine. TFEB expression was analyzed by Western blot. Representative of 4 repeats. Quantified in Fig. S4e. See also Fig. S4f.

(h) NIH 3T3 cells were transfected with *siOdc* to deplete endogenous spermidine and meanwhile treated with spermidine alone or in combination with *siDhs* transfection. TFEB expression was analyzed by Western blot. Representative of 3 repeats. See also Fig. S4g and S4h.

Figure 4 Hypusinated eIF5A assists polyproline synthesis in B cells.

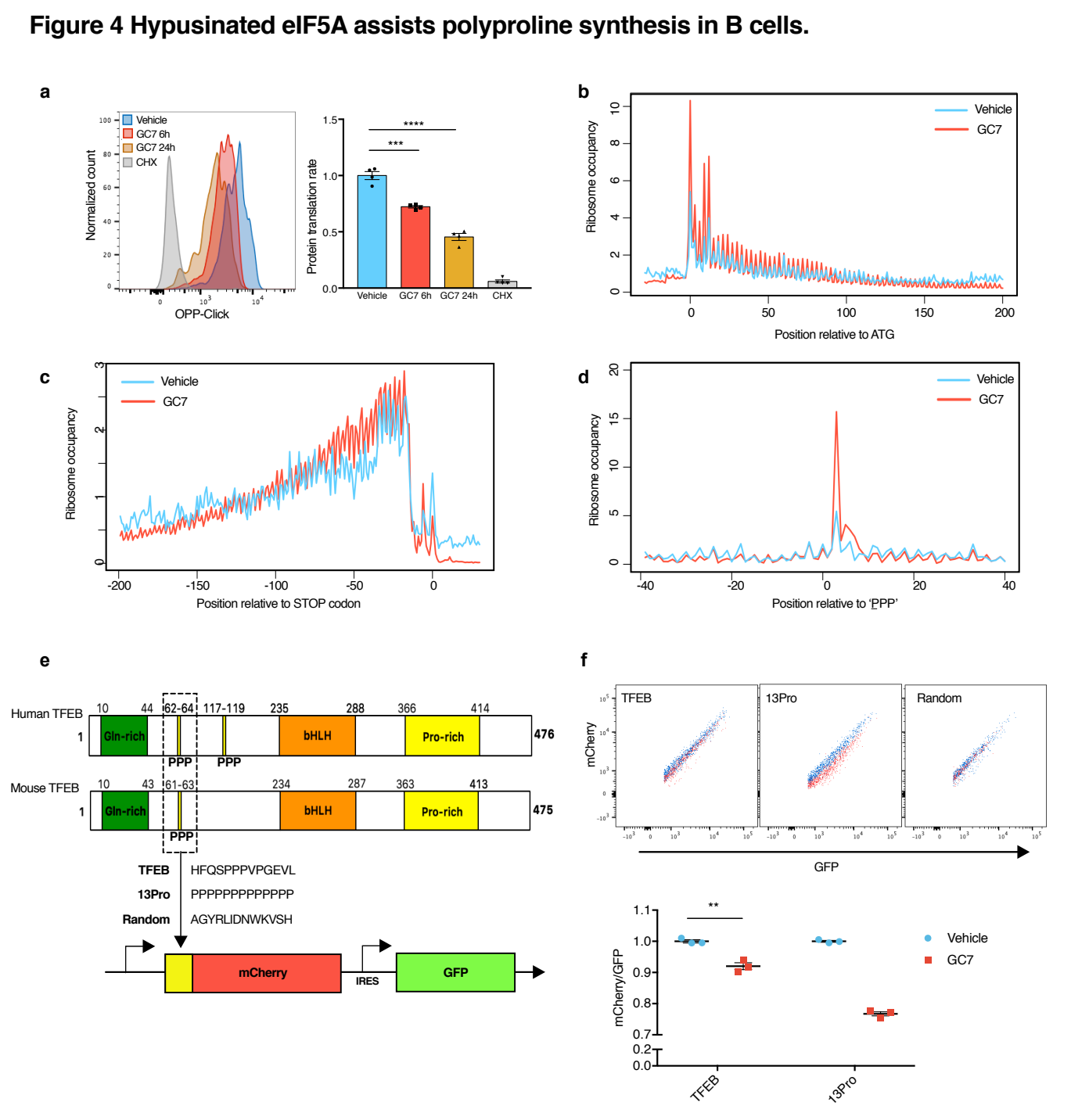

Figure 4. Hypusinated eIF5A assists polyproline synthesis in B cells.

(a) Jurkat cells were cultured with 100 μM GC7 for the indicated time or with the protein translation inhibitor cycloheximide (CHX) as control for 2 h. The relative protein translation rate was measured by OPP-Click assay with flow cytometry and normalized to Vehicle. n = 4. One-way ANOVA with post hoc Dunnett's test comparing with Vehicle. See also Fig. S5a.

(b-d) Murine B cells were treated with 10 μM GC7 as in Fig. 2i and processed for ribosome profiling. Ribosome occupancy of all genes is aligned at the start codon (b) or stop codon (c) and normalized to a mean value of 1 for each gene. (d) 100 genes with highest stalling ratio at triproline (PPP) motifs with or without GC7 are aligned with the underlined Pro on the P site of the ribosome.

(e) The polyproline motif of TFEB with its surrounding sequence was inserted before mCherry to report on protein translation. GFP after IRES is used to report on transfection. 13 consecutive prolines (13Pro) were used as positive control for translational stalling, while 13 random amino acids (Random) were used as negative control

(f) GC7-pretreated NIH 3T3 cells were transfected with the plasmids in e for 24 h. The expression of GFP and mCherry was measured by flow cytometry (upper panel). The ratio of geometric mean intensity mCherry/GFP was normalized to the average of Vehicle first and then to the Random negative control (lower panel). n = 3. Student's t-test.

Data represented as mean ± SEM. **P≤0.01, ***P≤0.001, ****P≤0.0001.

conserved function of eIF5A across kingdoms. Interestingly both human and mouse TFEB have at least one triproline motif (Fig. 4e). Moreover, sequences around this triproline are also ribosome-pausing motifs (SPP and PPV)[24], suggesting that this triproline-containing motif may confer TFEB the specific requirement to rely on eIF5A for smooth translation. Therefore, we examined if the triproline motif in mouse/human TFEB is sufficient to affect the translation rate of TFEB as regulated by hypusinated eIF5A. We generated three different constructs, using mCherry expression to report on the translation of either 13 amino acids containing the mouse TFEB triproline motif, 13 consecutive prolines or a random sequence of 13 amino acids (Fig. 4e). After transfection into NIH 3T3 cells, we measured translation using the ratio of the reporter mCherry to the transfection control GFP (Fig. 4f). As expected, the ratio of mCherry/GFP was not altered by GC7 for the random sequence, while the translation of 13 prolines was significantly downregulated by GC7. The translation of the TFEB triproline motif was also inhibited significantly, albeit less strongly (Fig. 4f). This data suggests that hypusination of eIF5A facilitates the translation of the transcription factor TFEB via its triproline motif.

Hypusination of eIF5A is essential for B-cell development and activation.

eIF5A and its hypusination are essential for cellular growth in cultured cells[28] and early embryonic development in mice[29], but its tissue-specific function is still unclear, although inducible whole-body knockout of *Dhs* in mice leads to a fatal wasting syndrome[30]. To investigate the function of hypusinated eIF5A during B cell development and activation *in vivo*, we generated competitive mixed bone marrow chimeras with inducible deletion of the hypusinating enzyme DHS. *Dhs* deletion was induced after long-term engraftment and B cell lineage reconstitution of CD45.2$^+$ cells were examined on day 8 and 30 after deletion (Fig. 5a, S6a and S6b). Percentages of CD45.2$^+$ of both transitional and mature follicular circulating B cells in peripheral blood were significantly affected by *Dhs* deletion on day 30 (Fig. 5b). Upon sacrifice of the mice on day 34 we investigated if this was due to a loss of progenitors in the bone marrow. Unexpectedly, all multipotent hematopoietic progenitors investigated (HSC, MPP, LMPP, LSK) were severely affected by DHS depletion (Fig. 5c). This is in line with a bone marrow hypocellularity reported previously in whole body *Dhs* knockout mice[30]. Consistent with depleted HSCs, splenic CD45.2$^+$ myeloid cells, which mostly lack self-renewal capacity and rely on replenishment from progenitor cells, were also severely depleted after *Dhs* deletion (Fig. S6c). Similarly, early B cell progenitors, newly formed B cells and follicular mature B cells from bone marrow as well as splenic transitional, marginal zone and follicular B cells were found significantly diminished (Fig. 5d and 5e). We checked if the remaining CD45.2$^+$ cells were indeed deleted for *Dhs* in blood (Fig. S6d), bone marrow and spleen (Fig.S6e). This analysis revealed that whilst on day 8 after deletion with Tamoxifen,

Figure 5 Hypusination of eIF5A is essential for B-cell development and activation.

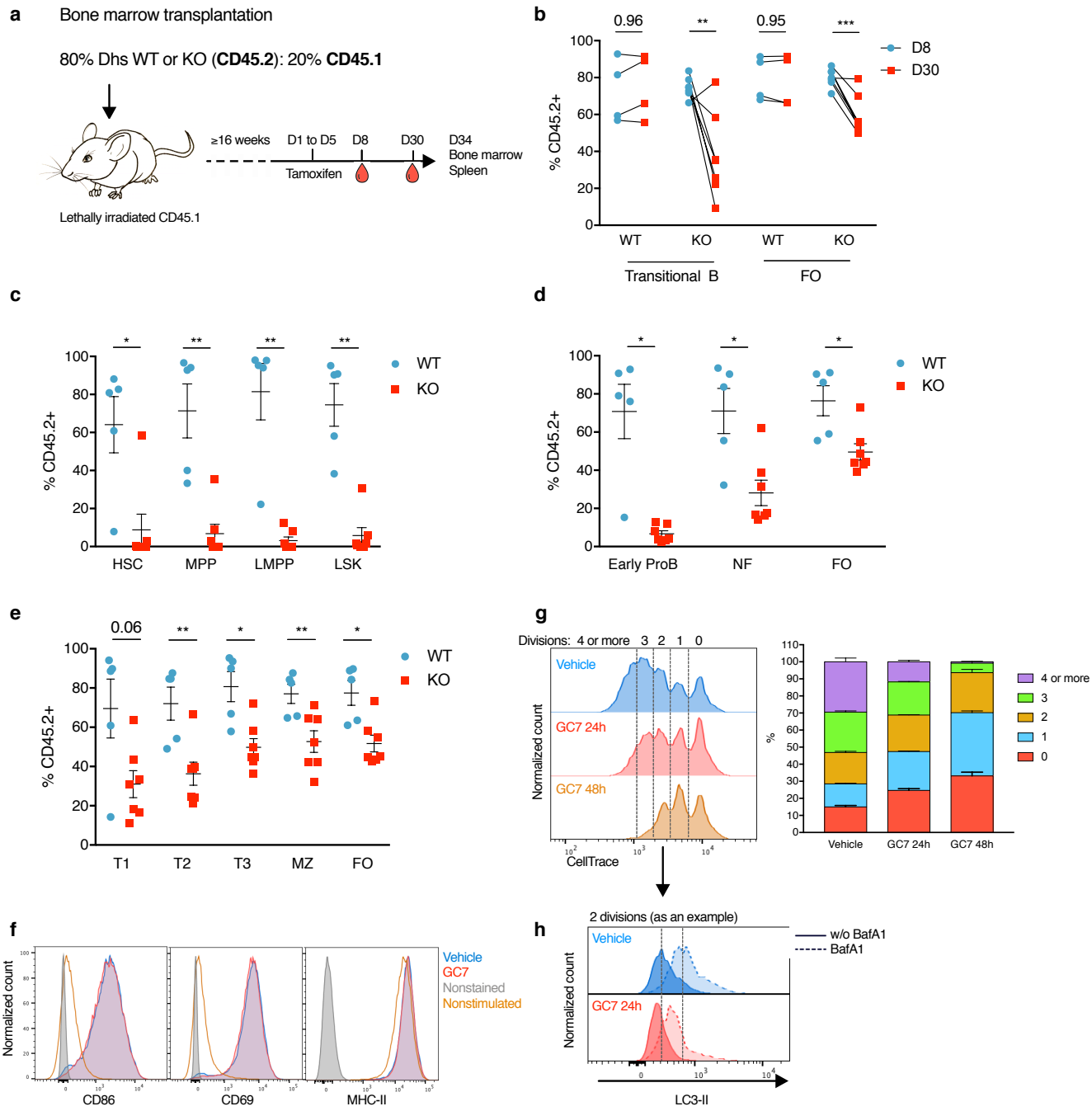

Figure 5. Hypusination of eIF5A is essential for B-cell development and activation.

(a-e) Competitive bone marrow chimeric mice were generated by transplanting bone marrow cells from tamoxifen-inducible CD45.2$^+$ *Dhs* knockout mice (WT: CAG-Cre/Esr1$^+$, *Dhs*$^{+/+}$; KO: CAG-Cre/Esr1$^+$, *Dhs*$^{f/f}$,) and wild type CD45.1$^+$ competitors into wild type CD45.1$^+$ recipient mice (a). After ≥ 16 weeks of long-term reconstitution, tamoxifen was administered by oral gavage for 5 consecutive days, followed with lineage contribution assessment in peripheral blood (b), bone marrow (c/d), and spleen (e). (b) The contribution of CD45.2$^+$ cells to transitional (CD19$^+$CD93$^+$) and mature follicular (FO) B cells (CD19$^+$CD93$^-$) in peripheral blood on day 8 and day 30 post tamoxifen induction was assessed by flow cytometry. (Gating strategy in Fig. S6a). n = 4-7 mice as indicated by dots. Two-way ANOVA with post hoc Sidak's test for transitional B cells and follicular B cells separately. (c-e) The contribution of CD45.2$^+$ cells to bone marrow haematopoietic stem and progenitor cells (c), early B cell progenitors (Early ProB, Hardy fraction A), newly formed B cells (NF, fraction E), follicular B cells (FO, fraction F) (d), and spleen transiational B cells (T1-3), marginal zone B cells (MZ) and follicular B cells (e) was assessed by flow cytometry on day 34 post tamoxifen induction. (Gating strategy of e is shown in Fig. S6b). n = 5-7 mice as indicated by dots. Welch's t-test. See also Fig. S6c-f.

(f) Wild type murine B cells were stimulated with 10 μg/mL LPS for 1 day with or without 10 μM GC7. The expression of early activation markers CD86, CD69, and MHC II was assessed by flow cytometry. Quantified in Fig. S6g.

(g/h) Wild type murine B cells were stained with CellTrace and cultured with LPS for 3 days. (g) 10 μM GC7 was added 24 h or 48 h before harvest for cell proliferation analysis. The percentage of cells that divided for the indicated times is quantified. n = 6 mice. (h) To measure autophagy, BafA1 was added 2 h before harvest followed by LC3-II flow cytometry staining. Quantified in Fig. S6h.

Data represented as mean ± SEM. *P≤0.05, **P≤0.01, ***P≤0.001.

blood cells were adequately deleted in the floxed *Dhs* mice, in cells that survived to day 34, *Dhs* was not deleted in most mice (Fig. S6e). The overall cellularity in bone marrow and spleen was not affected despite of the reduced CD45.2^{+} cell numbers (Fig. S6f), indicating that the remaining CD45.1^{+} and non-deleted CD45.2^{+} cells expanded and filled up the niche. The data together demonstrates a profound requirement of the eIF5A pathway in hematopoiesis and long-term survival of mature B cells.

To circumvent the defects of hematopoiesis and assess the role of eIF5A hypusination in B cell activation, we further attempted to delete *Dhs* after the first immunization with NP-CGG in *Dhs* KO bone marrow chimeric mice supported with Rag$^{-/-}$ bone marrow cells (to provide wild type hematopoietic cells for the survival of the mice, without T and B cells). As before, after 3 weeks of deletion, all remaining lymphocytes expressed wild type *Dhs* only. Levels of NP-specific IgG1 post-boost were not significantly changed in KO mice (data not shown), which can be attributed to contamination from non-deleted memory B cells. Overall the data implies that complete inhibition of eIF5A hypusination kills hematopoietic cells, and its effect on generation of antibodies cannot easily be investigated *in vivo* due to a) the rapid elimination of cells knocked out for *Dhs* and b) the limiting deletion efficiency in mature B cells with inducible deletion models.

To investigate if eIF5A has an effect on B cell activation, we induced B cell activation *ex vivo* with LPS while inhibiting hypusination with GC7. The up-regulation of early activation markers, including CD86, CD69, and MHC-II (Fig. 5f and S6g) were not changed upon GC7 treatment, indicating that hypusinated eIF5A does not regulate early activation signaling pathways. However, activation-induced cell proliferation was severely impaired upon inhibition of hypusinated eIF5A (Fig. 5g) in a time-dependent fashion, in line with the known function of eIF5A in supporting cellular growth[28]. Moreover, autophagy was reduced by GC7 treatment in B cells that had undergone 1, 2, or 3 divisions (Fig. 5h and Fig. S6h), i.e. when they were in their most proliferative phase. Taken together, these results indicate that the novel pathway identified here is not required for the signaling pathway immediately downstream of the LPS sensor TLR4, but is required for more distal signaling events, leading to proliferation, and other events for which autophagy might be required such as synthesis of immunoglobulins.

Spermidine induces TFEB expression and improves the function of old human B cells.

To investigate if this pathway regulates aging in human B cells, we firstly measured the levels of hypusinated eIF5A and TFEB in peripheral blood mononuclear cells (PBMCs) from

healthy donors of different ages. We found that PBMCs from donors aged 65 and over show a distinct reduction of TFEB protein. In some aged donors TFEB was even undetectable by Western blot (Fig. 6a). Splenocytes from old mice also show a distinct loss of TFEB (Fig. 6b), correlating with the reduced autophagic flux in Fig. 1b-1d. Furthermore hypusinated eIF5A and overall eIF5A were significantly diminished in human PBMCs from donors ≥65, although not as profoundly as TFEB (Fig. 6a). Using mass spectrometry, we show that endogenous spermidine in human PBMCs declines with age (Fig. 6c) as reported[31]. Next, we investigated whether TFEB is translationally regulated by spermidine and eIF5A in human primary B cells. Human B cells from young donors stimulated with anti-IgM and CD40L and treated with DFMO (to deplete endogenous spermidine levels) showed reduced hypusinated eIF5A and TFEB levels. Addition of spermidine rescued both proteins back to baseline (Fig. 6d).

Lastly and most importantly, we tested if spermidine improves old human B cell responses. The levels of both hypusinated eIF5A and TFEB (Fig. 6e), as well as autophagic flux (Fig. 6f) were significantly restored by spermidine treatment in B cells from aged donors in which spermidine levels are naturally low. IgG production by B cells from aged donors was also improved (Fig. 6g). Thus, replenishment of spermidine in B cells from aged donors rejuvenated their function.

This novel autophagy signaling pathway via eIF5A and TFEB and its involvement in immune senescence is summarized in Fig. 7.

Discussion

This study demonstrates that autophagic flux is regulated translationally. We identified the precise mechanism of this regulation, whereby the metabolite spermidine is a substrate for the hypusination of the translation factor eIF5A, which in turn controls the translation of TFEB via its triproline motif. This mechanism operates normally in young B cells, in which spermidine is abundant. In old B cells, however, replenishing spermidine levels restored this pathway, thereby rejuvenating responses and function *in vivo* in mice and *in vitro* in human. Depleted spermidine levels and subsequent low TFEB expression may be an important cause of the reduction in autophagy in the aging adaptive immune system, as well as in other tissues.

Not much is known about translation in lymphocytes except for a few pioneering studies in T[19, 32] and B cells[33]. Naïve B cells are in a metabolically quiescent state, with low protein translation (eIF5A expression) and autophagy, both of which are quickly up-regulated after activation. Autophagy and the translation machinery may form a regulatory loop to support

Figure 6 Spermidine induces TFEB expression and improves the function of old human B cells.

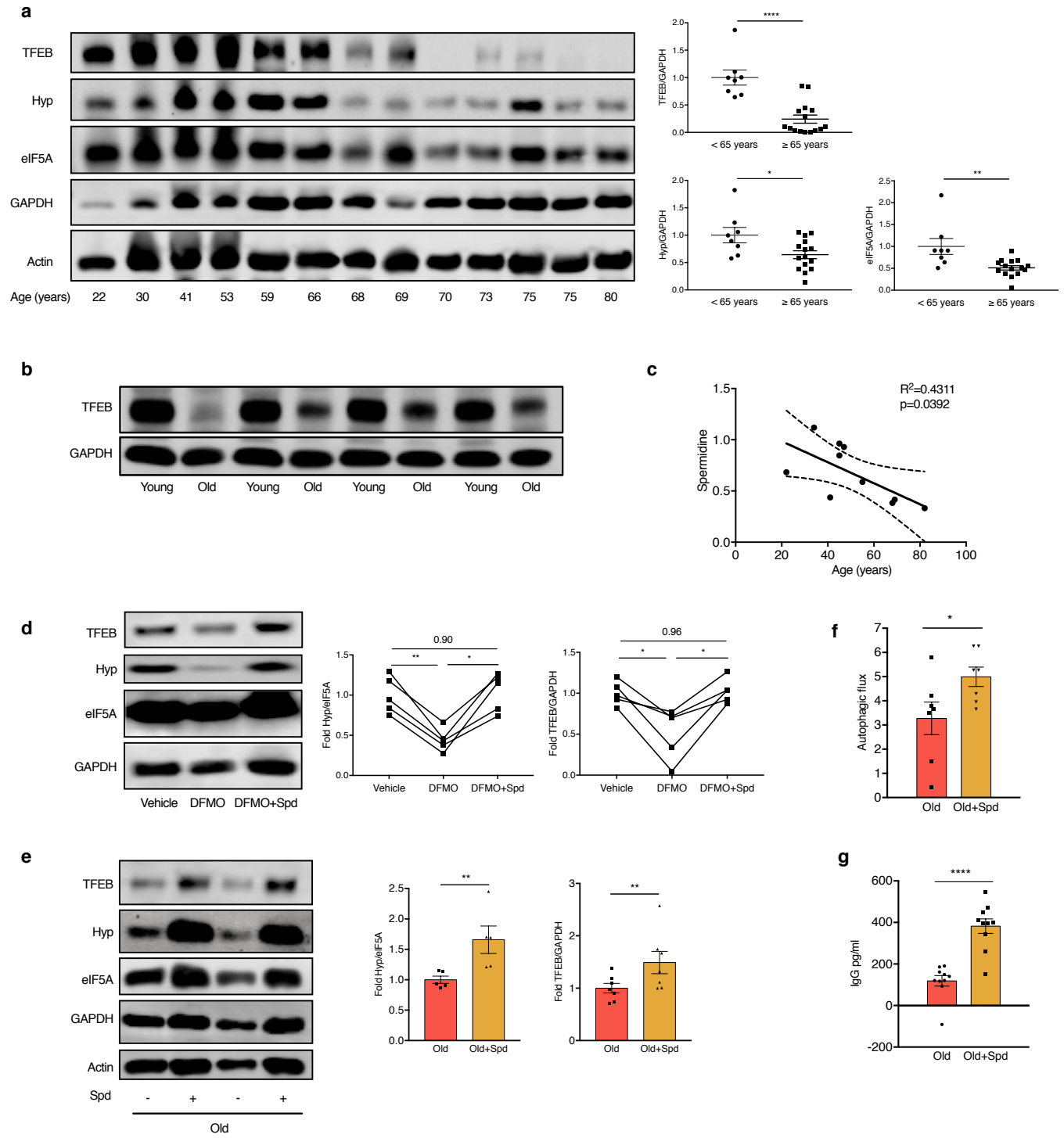

Figure 6. Spermidine induces TFEB expression and improves the function of old human B cells.

(a) The protein levels of TFEB, hypusinated eIF5A, and total eIF5A of PBMCs from healthy human donors of indicated ages were assessed by Western blot. A representative plot (left) and quantifications (right) are shown. Target band intensity was normalized to GAPDH first and then to the average of the < 65 years group. n = 8 (<65 years) or 15 (≥65 years) donors as indicated by dots. Student's t-test.

(b) The protein level of TFEB in B cells purified from young or old mice was measured by Western blot.

(c) Spermidine content of PBMCs collected from healthy donors was measured by GC-MS. Linear regression with 95% confidence intervals. The goodness of fit was assessed by R^2. The P value of the slope is calculated by F test. n = 10 donors as indicated by dots.

(d) Sorted B cells from young human donors were cultured with anti-IgM and CD40L for 7 days treated with DFMO alone or together with 10 μM spermidine. The level of TFEB and eIF5A hypusination was measured by Western blot. The representative plot and quantifications are shown. n = 5 donors as indicated by dots. Paired one-way ANOVA with post hoc Tukey's test.

(e-g) Sorted B cells from old human donors (age 77.5 ± 6.3 years) were cultured as in B together with 10 μM spermidine. (e) The protein levels of TFEB and eIF5A hypusination were measured by Western blot. Target band intensity was normalized to eIF5A (for Hyp) or GAPDH (for TFEB) first and then to the average of the Old group. n = 5 (Hyp/eIF5A) or 7 (TFEB/GAPDH) donors. (f) Autophagic flux was measured by flow cytometry as in Fig. 1a/b. n = 7 donors. (g) Supernatant IgG was assessed by ELISA. n=10 donors. Paired one-tailed (e) or two-tailed (f/g) t-test.

Data represented as mean ± SEM. *P≤0.05, **P≤0.01, ***P≤0.001, ****P≤0.0001.

Figure 7. Proposed working model of a novel autophagy signaling pathway and its involvement in ageing.

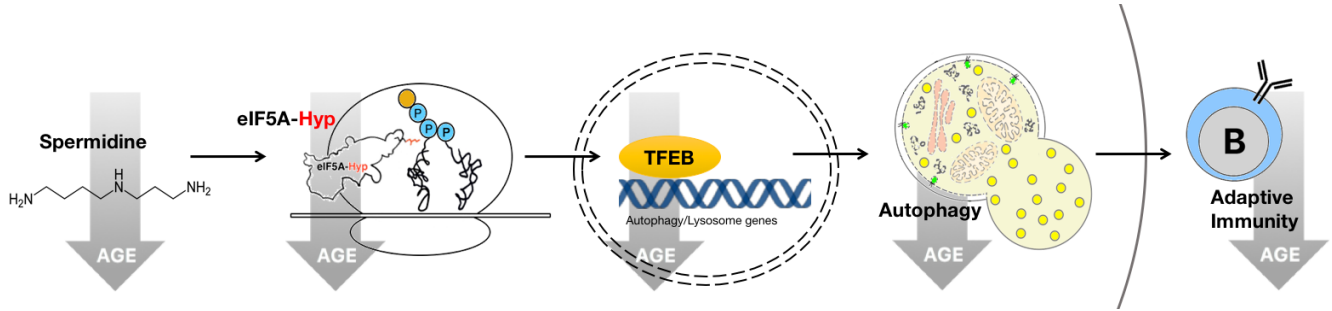

Figure 7. Proposed working model of a novel autophagy signaling pathway and its involvement in ageing.

Spermidine is a unique substrate for the hypusination of eIF5A. Hypusinated eIF5A regulates TFEB expression at the translational level. TFEB is a master transcription factor of autophagy, which is required for long-term adaptive immune responses. Spermidine levels, hypusinated eIF5A, TFEB, autophagy, and adaptive immunity are reduced with age, and spermidine administration rejuvenates B cell responses in both mouse and human.

the metabolic requirements of proliferation and immunoglobulin production following activation. In this loop, autophagy provides substrates and energy for translation, while increased translation induces the synthesis of certain autophagic proteins such as TFEB. Specifically, a particular requirement for rapid provision of amino acids and unfolded protein degradation by autophagy may exist in long-lived plasma cells, which secrete antibodies at the rate of about 2,000 molecules per second[5, 34]. It has also been shown recently that another autophagy protein, ATG3 is regulated by eIF5A in HeLa cells[35], suggesting that both regulatory proteins (such as TFEB) and structural proteins (such as ATG3) in the autophagy pathway can be regulated at the protein translational level. However, in our study we could not find a reduction of ATG3 when eIF5A hypusination was inhibited in primary B cells by proteomics (Fig. 3a) or in Jurkat cells by western blot (data not shown). It is possible that ATG3 is preferentially regulated in HeLa cells by eIF5A.

The anti-aging function of TFEB seems to be highly conserved, found in mice and humans. Earlier studies found it to be a uniquely important transcription factor for lifespan extension in *C. elegans*[36]. Moreover, it is likely that the control of TFEB via translation is a broad, maybe universal mechanism, operating across many tissue types (here in NIH 3T3 cells, Jurkat lymphocytes and in mouse and human primary B cells). TFEB is known to be post-translationally controlled via (1) mTORC1-dependent phosphorylation for cytoplasmic retention, and (2) calcium-dependent dephosphorylation to signal for nuclear translocation[37]. We now add an mTOR-independent step of regulation at the level of translation. Interestingly, our data suggest that the eIF5A pathway controls translation of proteins containing PPP motifs, which are highly specific binding motifs with low affinity and as such a hallmark of transcription factors[38]. Moreover, importantly we also found that hypusinated eIF5A is critical in initiation, elongation, and termination of translation and its decrease with age may contribute to the global decrease in protein synthesis in senescent cells.

We have shown hypusinated eIF5A and TFEB levels are correlated with age in immune cells. Blood aging biomarkers are urgently needed to gauge the efficacy of new drugs that might prolong health span. Autophagy is one of the few general mechanisms that underpin many age-related diseases and is therefore a good target for anti-aging drugs. Lastly given that the translation factor eIF5A is regulated by post-translational modifications, mediated by enzymes, these can potentially be harnessed therapeutically.

Acknowledgments

We thank the staff of the University of Oxford Biomedical Services Unit for animal care, Jonathan Webber and Craig Waugh for assistance with FACS sorting, and Volodymyr Nechyporuk-Zloy for assistance with confocal microscopy imaging, Alfredo Castello Palomares for help with SILAC proteomics and providing general advice. Alexander Clarke is acknowledged for reading the manuscript. H.Z. is funded by the China Scholarship Council and Elysium Health fellowship and the A.K.S. lab is funded by a Wellcome Trust Investigator Award (103830/Z/14/Z). S.B. is funded by a Swiss National Science Foundation Grant (31003A_150066).). J.F. is funded by the Wellcome Trust Chromosome and Developmental Biology PhD Program (ALR00520). J.M. lab is funded by BBSRC grant (BB/P00296X/1). Li-Cor Odyssey imager is funded by ERC (AdG 670930).

Authors contributions

HZ designed and performed most experiments, GA performed human B cell studies, JF helped to set up and analyze ribosome profiling in primary B cells, PC and SM generated proteomic data, YS/LF ran some Western blots, SB provided KD/KO cell lines and Dhs KO bone marrow, TR helped to set up the Dhs KO chimera experiments, JM and SB gave advice on data interpretation and read manuscript, AKS supervised this project (HZ's thesis), designed the experiments, provided funds, and wrote the manuscript.

There are no financial competing interests.

References

1. Yoshikawa, T.T. Epidemiology and unique aspects of aging and infectious diseases. *Clin Infect Dis* **30**, 931-933 (2000).
2. Xu, X. *et al.* Autophagy is essential for effector CD8(+) T cell survival and memory formation. *Nature immunology* **15**, 1152-1161 (2014).
3. Puleston, D.J. *et al.* Autophagy is a critical regulator of memory CD8(+) T cell formation. *eLife* **3** (2014).
4. Chen, M. *et al.* Essential role for autophagy in the maintenance of immunological memory against influenza infection. *Nature medicine* **20**, 503-510 (2014).
5. Pengo, N. *et al.* Plasma cells require autophagy for sustainable immunoglobulin production. *Nature immunology* **14**, 298-305 (2013).
6. Pyo, J.O. *et al.* Overexpression of Atg5 in mice activates autophagy and extends lifespan. *Nature communications* **4**, 2300 (2013).
7. Fernandez, A.F. *et al.* Disruption of the beclin 1-BCL2 autophagy regulatory complex promotes longevity in mice. *Nature* (2018).
8. Bjedov, I. *et al.* Mechanisms of life span extension by rapamycin in the fruit fly Drosophila melanogaster. *Cell metabolism* **11**, 35-46 (2010).
9. Eisenberg, T. *et al.* Cardioprotection and lifespan extension by the natural polyamine spermidine. *Nature medicine* (2016).
10. Dever, T.E., Gutierrez, E. & Shin, B.S. The hypusine-containing translation factor eIF5A. *Critical reviews in biochemistry and molecular biology*, 1-13 (2014).
11. Settembre, C. *et al.* TFEB links autophagy to lysosomal biogenesis. *Science* **332**, 1429-1433 (2011).
12. Phadwal, K. *et al.* A novel method for autophagy detection in primary cells: impaired levels of macroautophagy in immunosenescent T cells. *Autophagy* **8**, 677-689 (2012).
13. Henry, C.J., Marusyk, A. & DeGregori, J. Aging-associated changes in hematopoiesis and leukemogenesis: what's the connection? *Aging* **3**, 643-656 (2011).
14. Eisenberg, T. *et al.* Induction of autophagy by spermidine promotes longevity. *Nature cell biology* **11**, 1305-1314 (2009).
15. Morselli, E. *et al.* Spermidine and resveratrol induce autophagy by distinct pathways converging on the acetylproteome. *The Journal of cell biology* **192**, 615-629 (2011).
16. Madeo, F., Eisenberg, T., Pietrocola, F. & Kroemer, G. Spermidine in health and disease. *Science* **359** (2018).
17. Sun, D. *et al.* Epigenomic profiling of young and aged HSCs reveals concerted changes during aging that reinforce self-renewal. *Cell stem cell* **14**, 673-688 (2014).
18. Rossi, D., Kuroshu, R., Zanelli, C.F. & Valentini, S.R. eIF5A and EF-P: two unique translation factors are now traveling the same road. *Wiley interdisciplinary reviews. RNA* **5**, 209-222 (2014).
19. Hukelmann, J.L. *et al.* The cytotoxic T cell proteome and its shaping by the kinase mTOR. *Nature immunology* **17**, 104-112 (2016).
20. Sardiello, M. *et al.* A gene network regulating lysosomal biogenesis and function. *Science* **325**, 473-477 (2009).
21. Xiao, Q. *et al.* Neuronal-Targeted TFEB Accelerates Lysosomal Degradation of APP, Reducing Abeta Generation and Amyloid Plaque Pathogenesis. *The Journal of neuroscience : the official journal of the Society for Neuroscience* **35**, 12137-12151 (2015).
22. Cambridge, S.B. *et al.* Systems-wide proteomic analysis in mammalian cells reveals conserved, functional protein turnover. *Journal of proteome research* **10**, 5275-5284 (2011).
23. Landau, G., Bercovich, Z., Park, M.H. & Kahana, C. The role of polyamines in supporting growth of mammalian cells is mediated through their requirement for translation initiation and elongation. *The Journal of biological chemistry* **285**, 12474-12481 (2010).
24. Schuller, A.P., Wu, C.C., Dever, T.E., Buskirk, A.R. & Green, R. eIF5A Functions Globally in Translation Elongation and Termination. *Molecular cell* **66**, 194-205 e195 (2017).
25. Woolstenhulme, C.J., Guydosh, N.R., Green, R. & Buskirk, A.R. High-precision analysis of translational pausing by ribosome profiling in bacteria lacking EFP. *Cell reports* **11**, 13-21 (2015).
26. Ude, S. *et al.* Translation elongation factor EF-P alleviates ribosome stalling at polyproline stretches. *Science* **339**, 82-85 (2013).
27. Doerfel, L.K. *et al.* EF-P is essential for rapid synthesis of proteins containing consecutive proline residues. *Science* **339**, 85-88 (2013).

28. Park, M.H., Wolff, E.C., Lee, Y.B. & Folk, J.E. Antiproliferative effects of inhibitors of deoxyhypusine synthase. Inhibition of growth of Chinese hamster ovary cells by guanyl diamines. *The Journal of biological chemistry* **269**, 27827-27832 (1994).
29. Nishimura, K., Lee, S.B., Park, J.H. & Park, M.H. Essential role of eIF5A-1 and deoxyhypusine synthase in mouse embryonic development. *Amino acids* **42**, 703-710 (2012).
30. Pallmann, N. *et al.* Biological Relevance and Therapeutic Potential of the Hypusine Modification System. *The Journal of biological chemistry* (2015).
31. Pucciarelli, S. *et al.* Spermidine and spermine are enriched in whole blood of nona/centenarians. *Rejuvenation Res* **15**, 590-595 (2012).
32. Tan, T.C.J. *et al.* Suboptimal T-cell receptor signaling compromises protein translation, ribosome biogenesis, and proliferation of mouse CD8 T cells. *Proceedings of the National Academy of Sciences of the United States of America* **114**, E6117-E6126 (2017).
33. Diaz-Munoz, M.D. *et al.* The RNA-binding protein HuR is essential for the B cell antibody response. *Nat Immunol* **16**, 415-425 (2015).
34. Clarke, A.J. *et al.* Autophagy is activated in systemic lupus erythematosus and required for plasmablast development. *Annals of the rheumatic diseases* **74**, 912-920 (2015).
35. Lubas, M. *et al.* eIF5A is required for autophagy by mediating ATG3 translation. *EMBO reports* (2018).
36. Lapierre, L.R. *et al.* The TFEB orthologue HLH-30 regulates autophagy and modulates longevity in Caenorhabditis elegans. *Nature communications* **4**, 2267 (2013).
37. Napolitano, G. & Ballabio, A. TFEB at a glance. *Journal of cell science* **129**, 2475-2481 (2016).
38. Morgan, A.A. & Rubenstein, E. Proline: the distribution, frequency, positioning, and common functional roles of proline and polyproline sequences in the human proteome. *PloS one* **8**, e53785 (2013).

Figure S1. Related to Figure 1. Spermidine does not affect hematopoiesis in old mice.

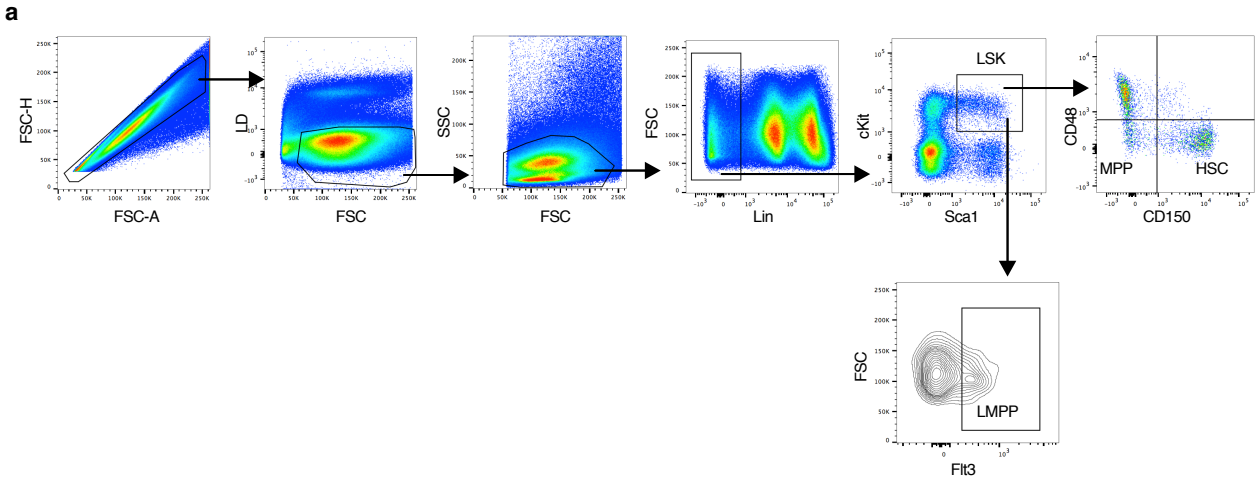

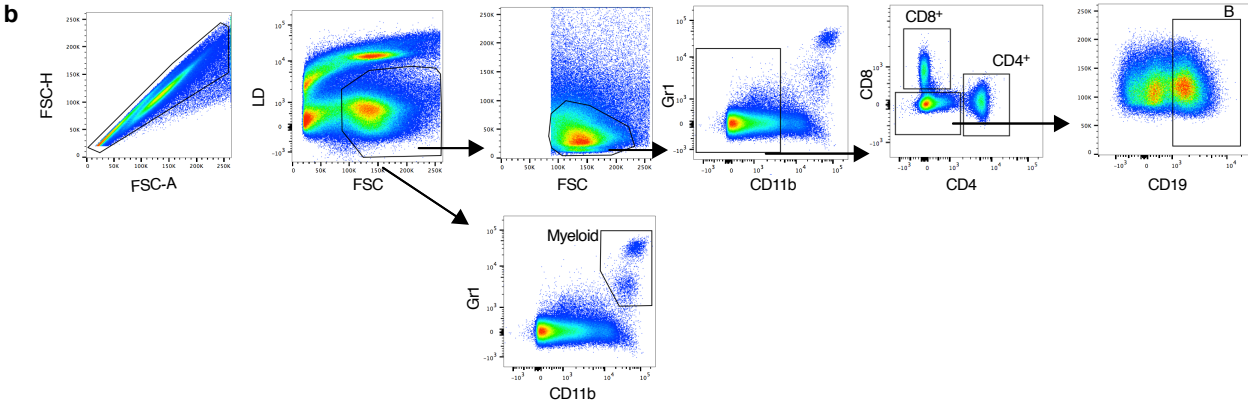

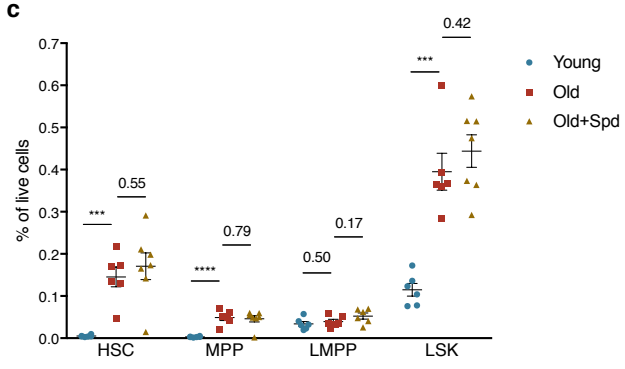

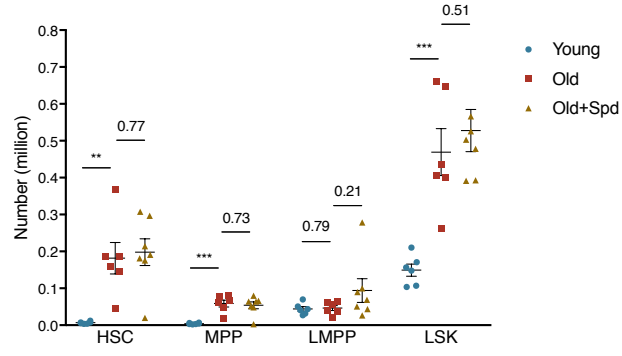

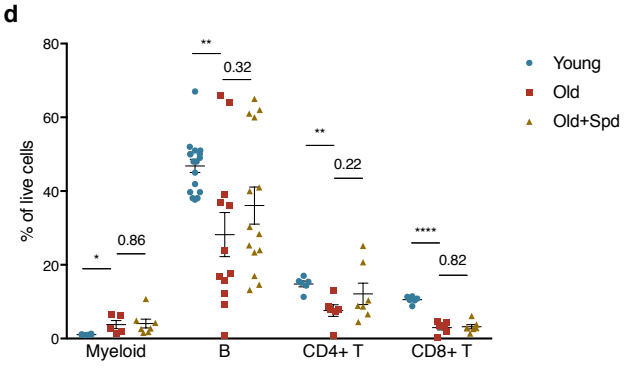

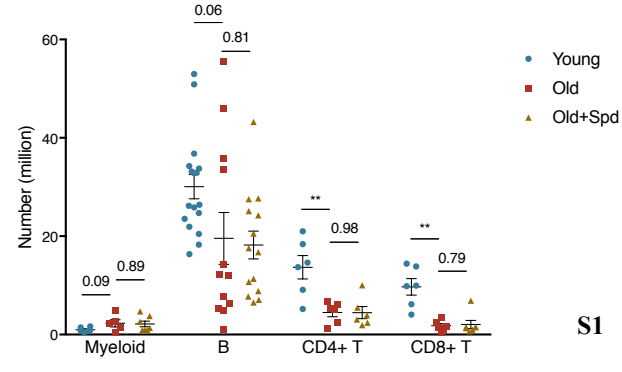

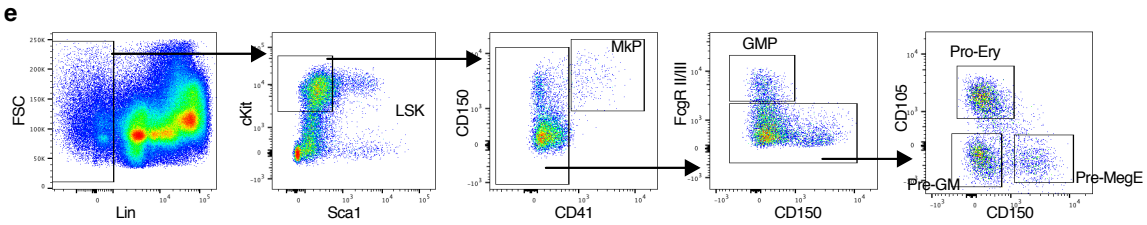
e
FSC
Lin
cKit
Sca1
LSK
CD150
CD41
MkP
FcgR II/III
CD150
GMP
CD105
CD150
Pro-Ery
Pre-GM
Pre-MegE

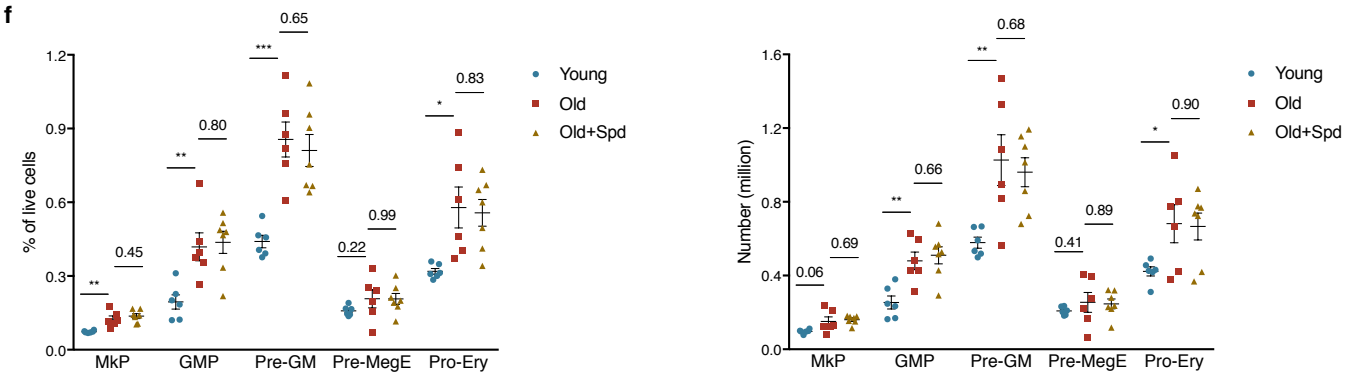
f
% of live cells
Young
Old
Old+Spd
MkP
GMP
Pre-GM
Pre-MegE
Pro-Ery
Number (million)

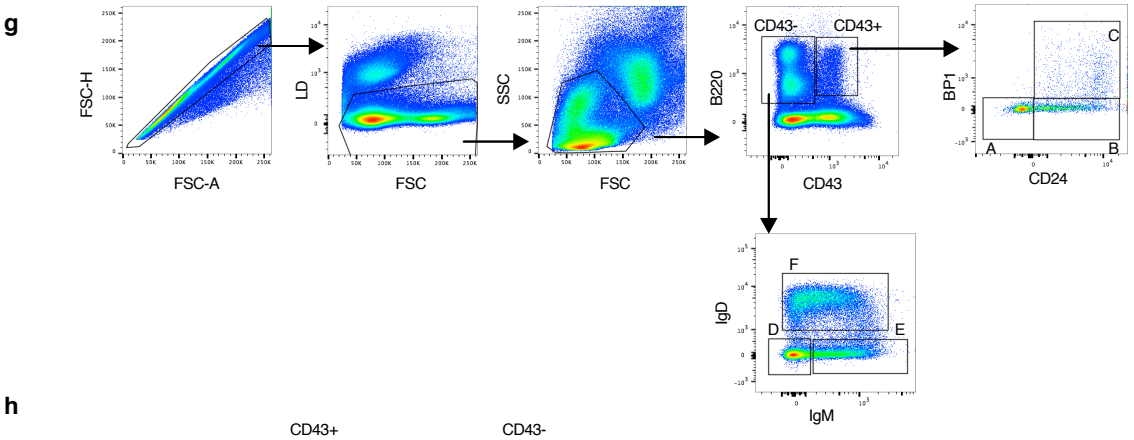
g
FSC-H
FSC-A
LD
FSC
SSC
FSC
CD43-
CD43+
B220
CD43
BP1
CD24
A
B
C
IgD
IgM
D
E
F

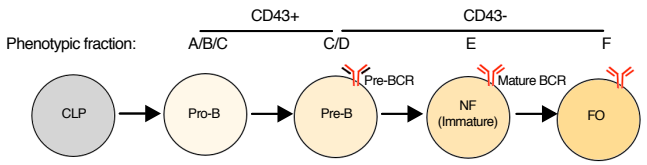
h
Phenotypic fraction:
CD43+
CD43-
A/B/C
C/D
E
F
CLP
Pro-B
Pre-B
Pre-BCR
NF
(Immature)
Mature BCR
FO

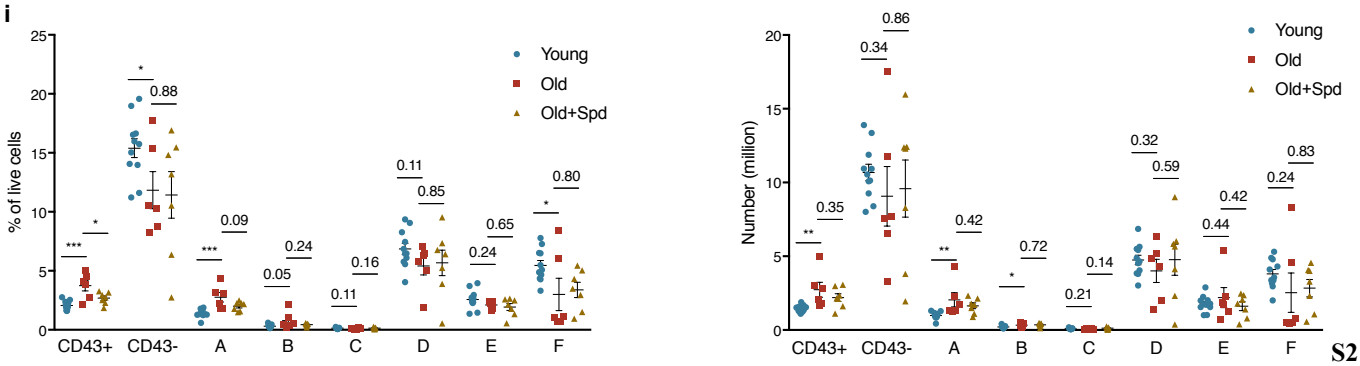
i
% of live cells
Young
Old
Old+Spd
CD43+
CD43-
A
B
C
D
E
F
Number (million)

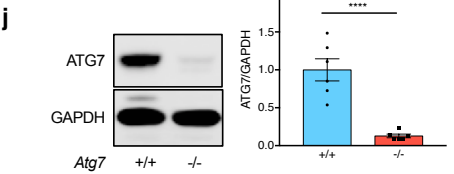
j
ATG7
GAPDH
Atg7 +/+ -/-
ATG7/GAPDH
2.0
1.5
1.0
0.5
0.0
****
+/+
-/-

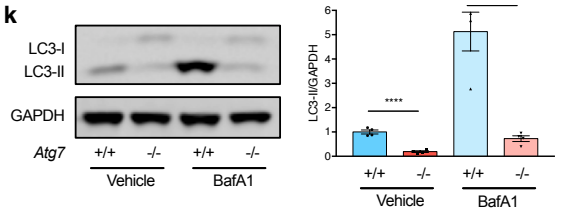
k
LC3-I
LC3-II
GAPDH
Atg7 +/+ -/- +/+ -/-
Vehicle
BafA1
LC3-II/GAPDH
6
5
4
3
2
1
0
****
***
+/+ -/- +/+ -/-
Vehicle
BafA1

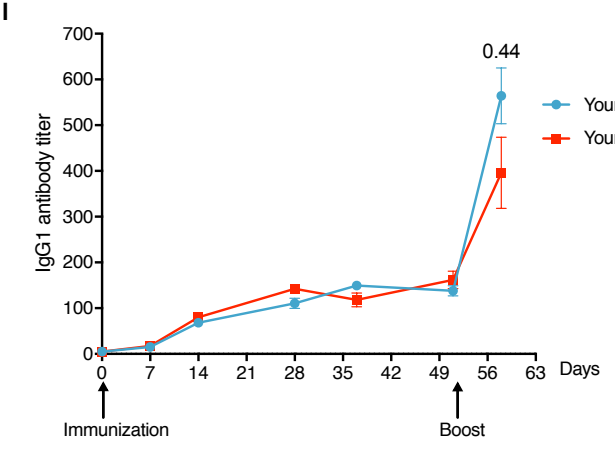
l
IgG1 antibody titer
700
600
500
400
300
200
100
0
0.44
Young
Young+Spd
0 7 14 21 28 35 42 49 56 63
Days
Immunization
Boost

Figure S2. Related to Figure 2. Spermidine does not directly inhibit HAT activities and high-dose spermidine induces cellular stress in Jurkat cells.

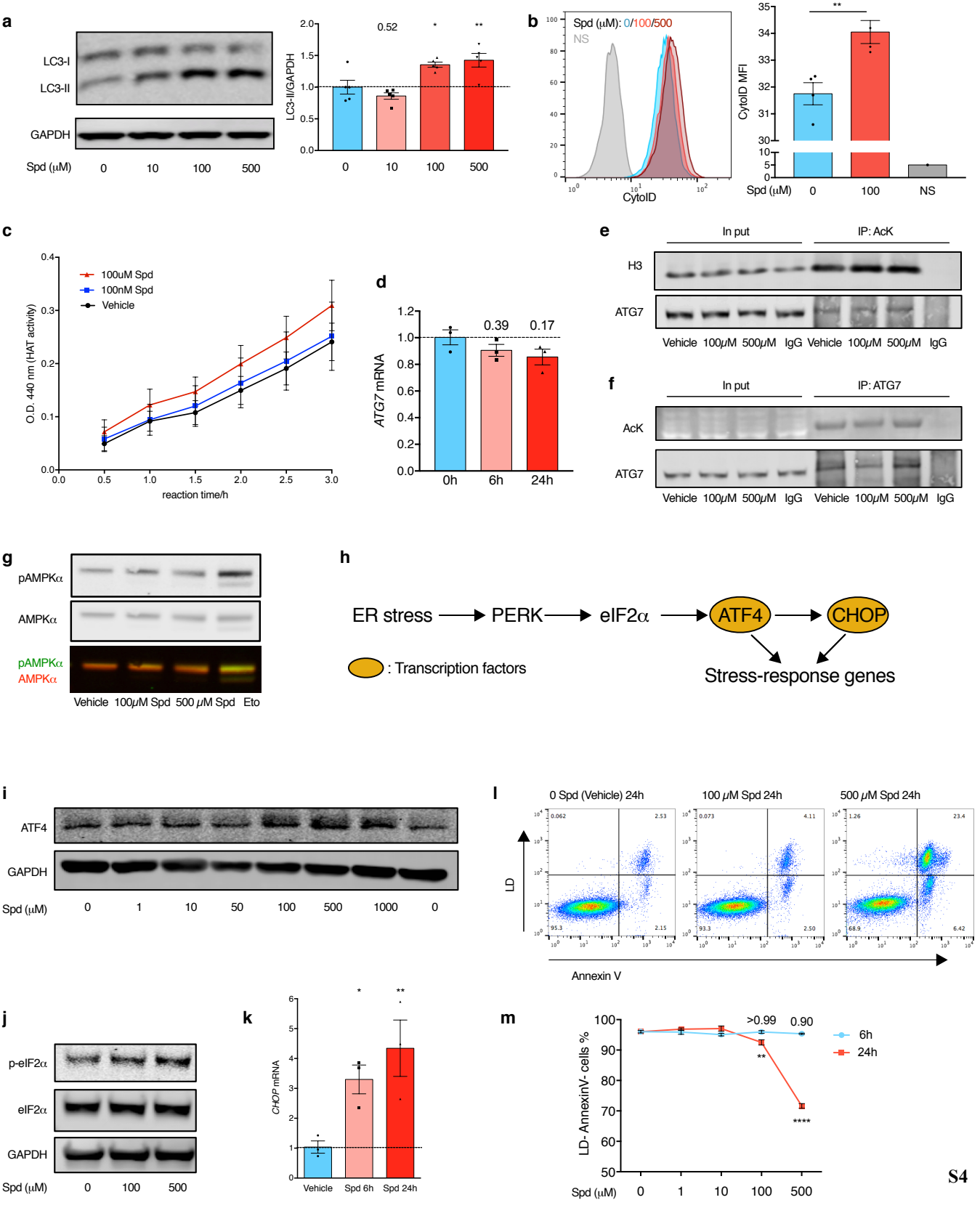

Figure S3. Related to Figure 2. Inhibition of eIF5A hypusination reduces autophagy.

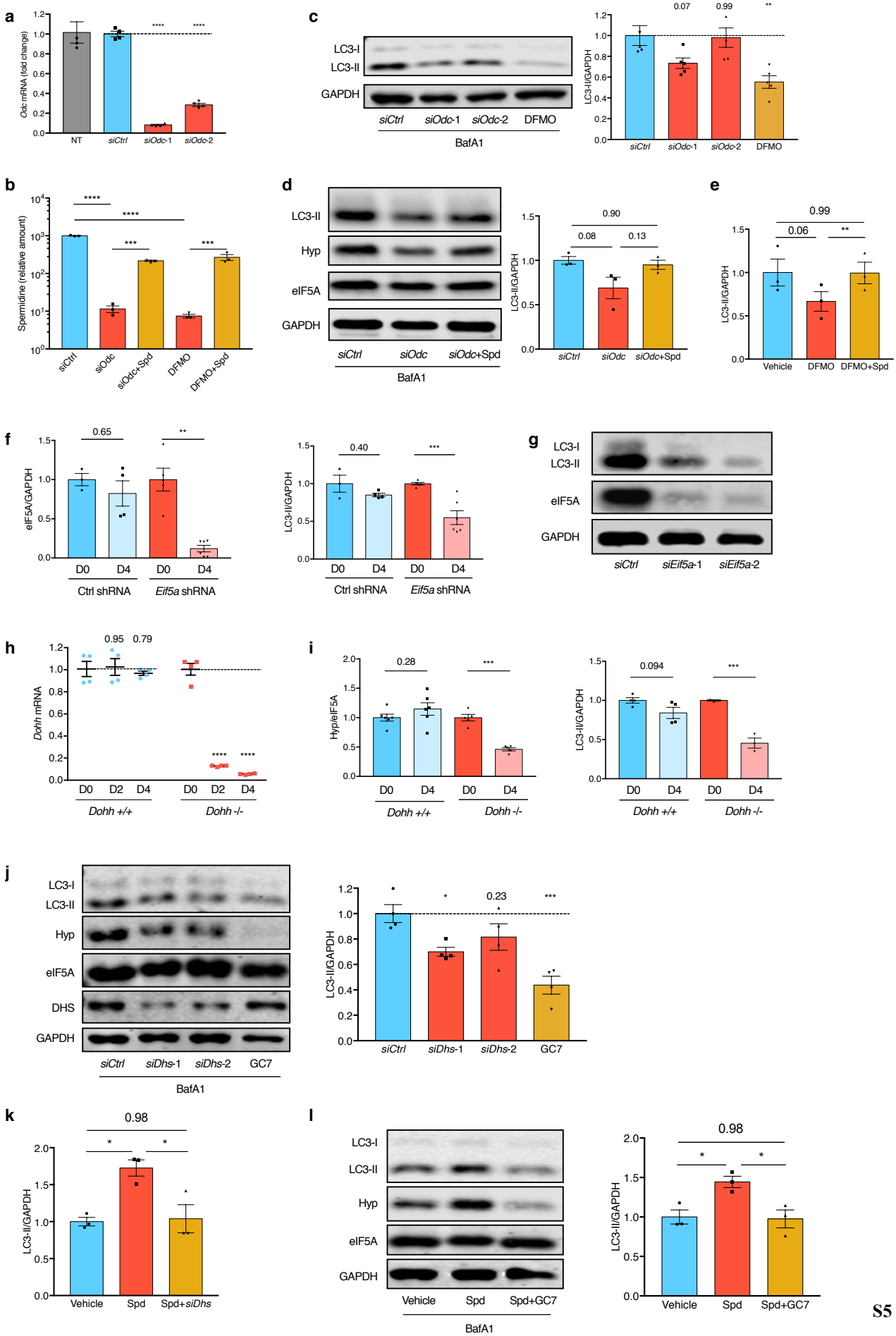

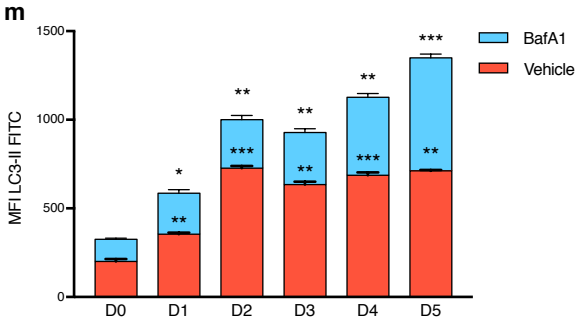
m
MFI LC3-II FITC
1500
1000
500
0
BafA1
Vehicle
D0
D1
D2
D3
D4
D5

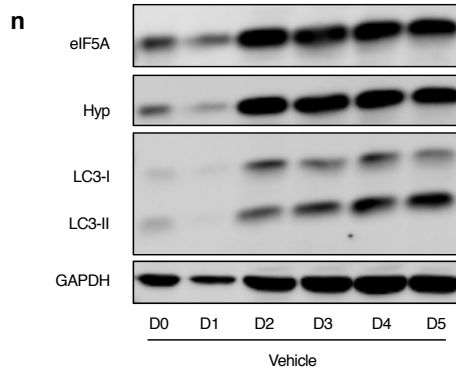
n
eIF5A
Hyp
LC3-I
LC3-II
GAPDH
D0
D1
D2
D3
D4
D5
Vehicle

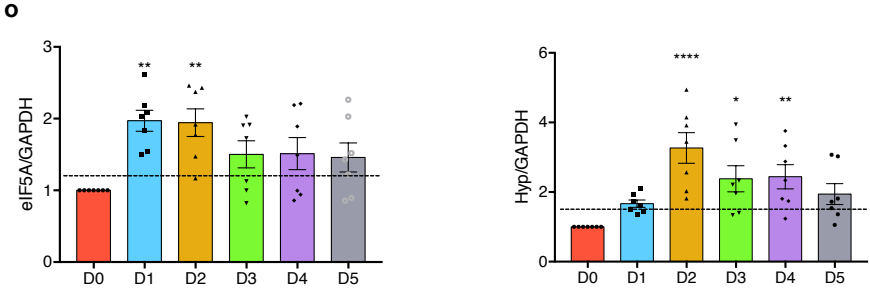
o
eIF5A/GAPDH
Hyp/GAPDH
D0
D1
D2
D3
D4
D5

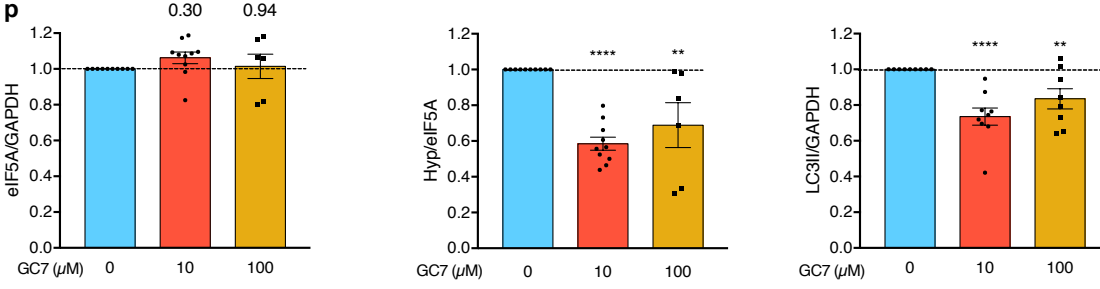
p
eIF5A/GAPDH
0.30
0.94
Hyp/eIF5A
LC3II/GAPDH
GC7 (μM)
0
10
100

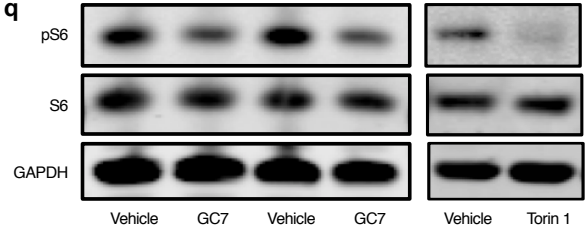
q
pS6
S6
GAPDH
Vehicle
GC7
Vehicle
GC7
Vehicle
Torin 1

S6

Figure S4. Related to Figure 3. eIF5A and its hypusination are required for TFEB expression.

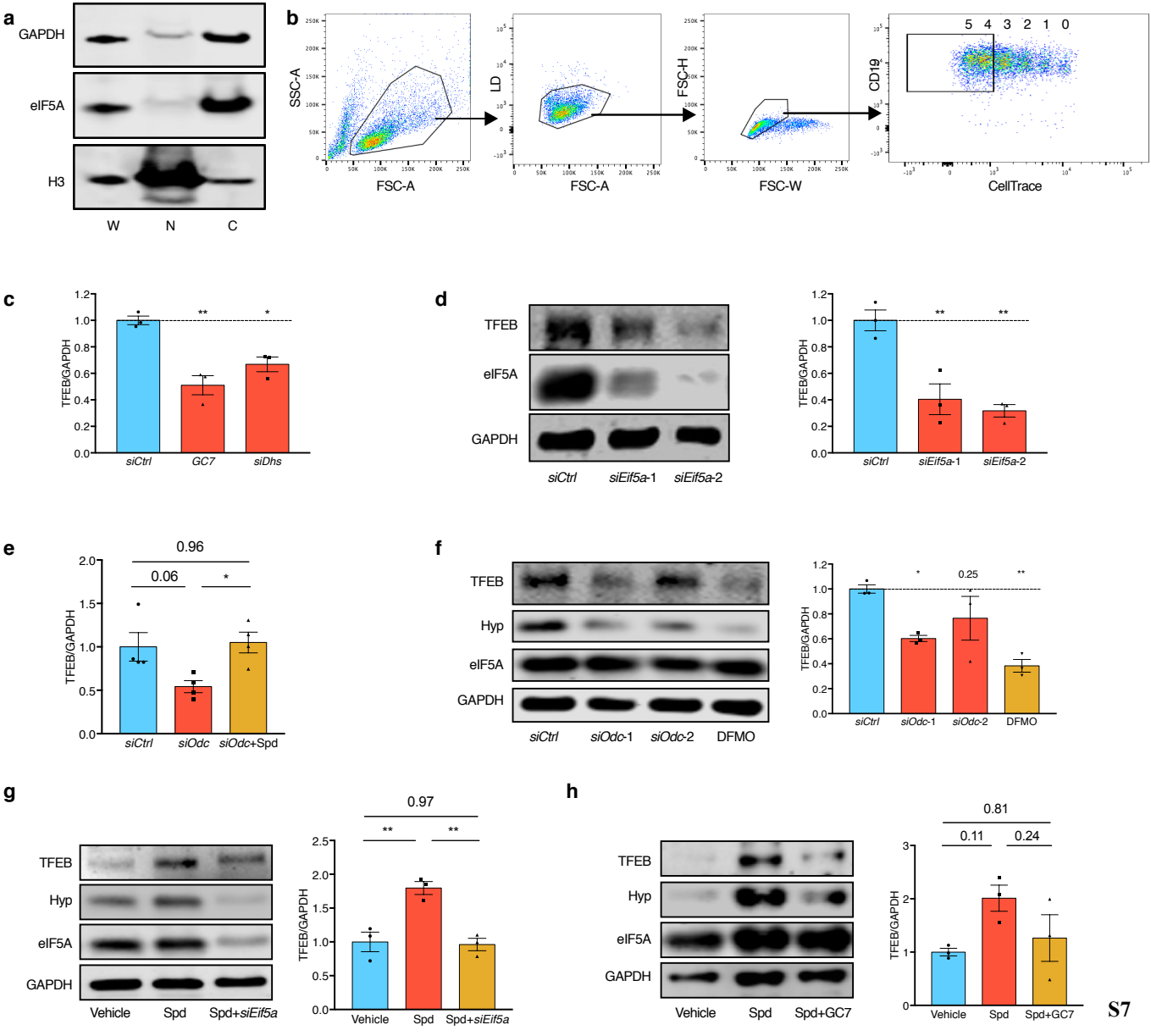

Figure S5. Related to Figure 4. Spermidine maintains protein synthesis.

a

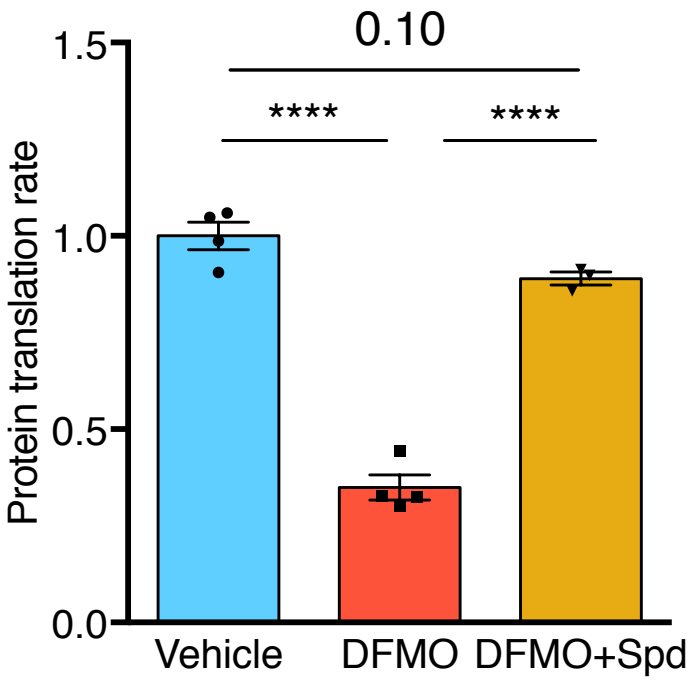

Figure S6. Related to Figure 5. Hypusinated eIF5A is essential for hematopoiesis and B cell activation.

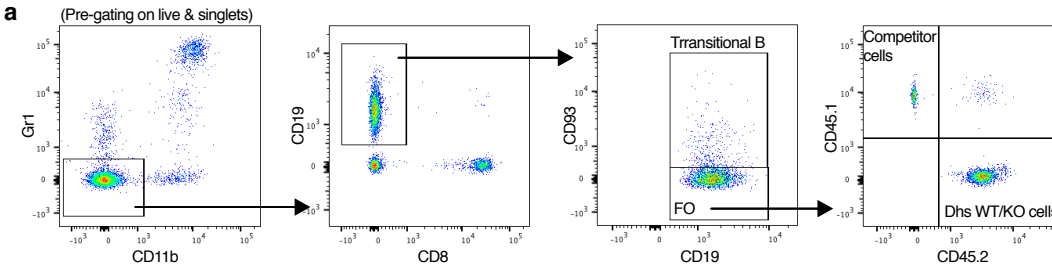

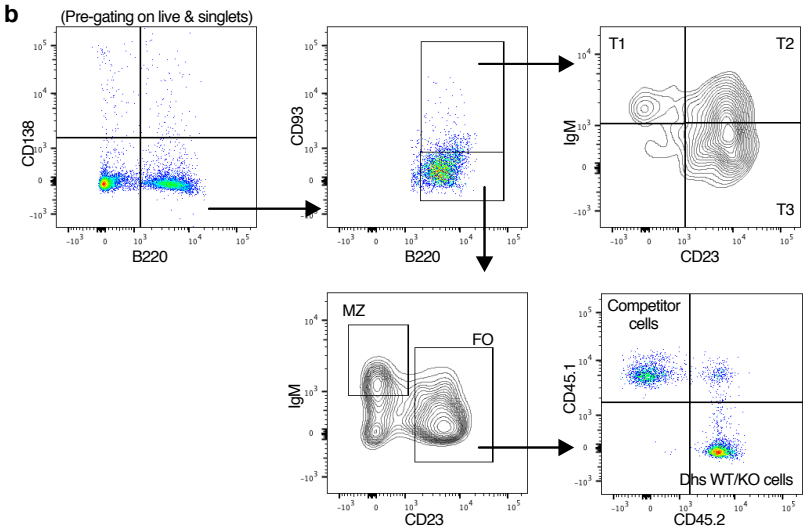

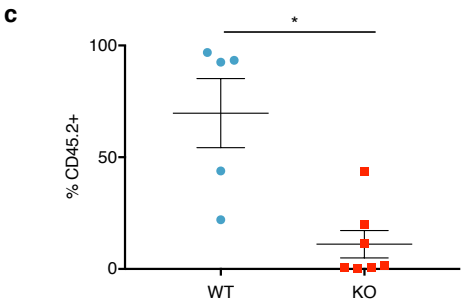

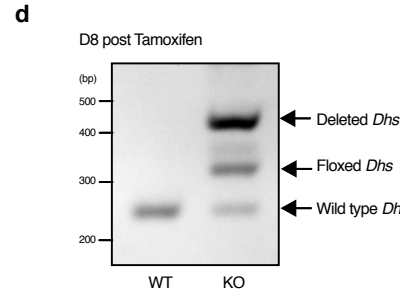

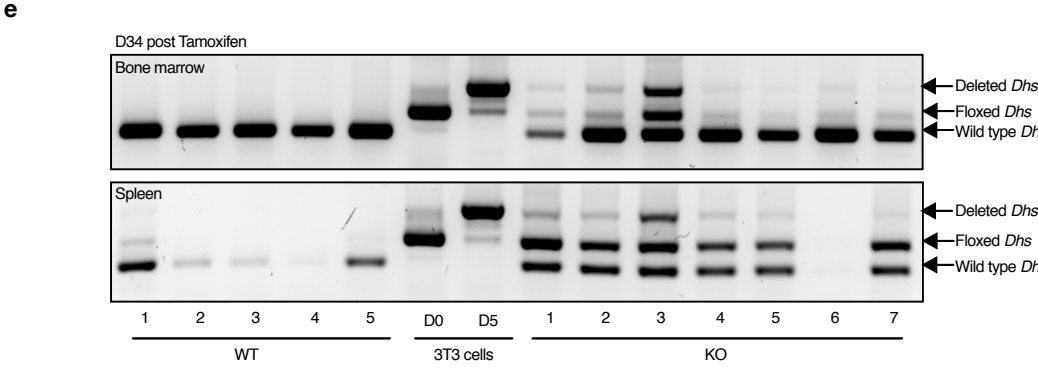

f

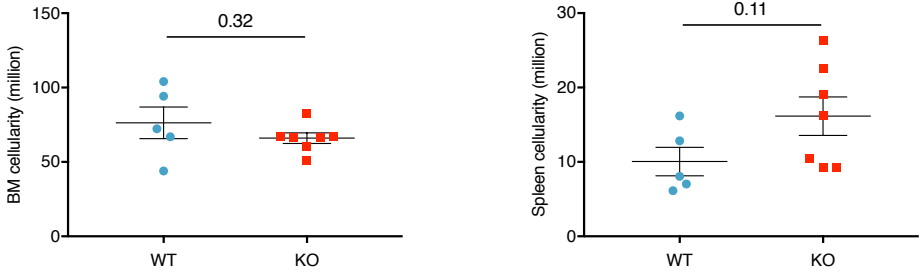
BM cellularity (million)
150
100
50
0
0.32
WT
KO
Spleen cellularity (million)
30
20
10
0
0.11
WT
KO

g

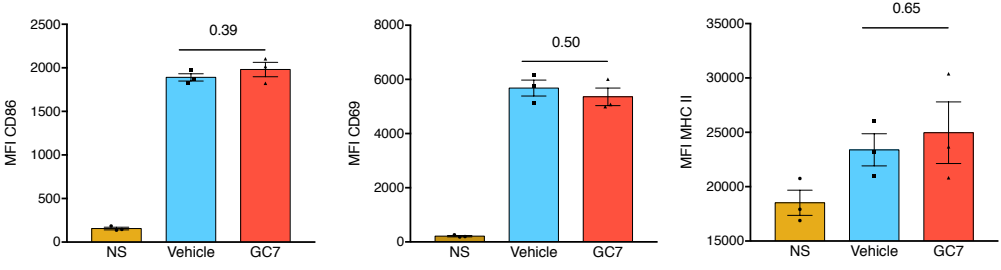
MFI CD86
2500
2000
1500
1000
500
0
0.39
NS
Vehicle
GC7
MFI CD69
8000
6000
4000
2000
0
0.50
NS
Vehicle
GC7
MFI MHC II
35000
30000
25000
20000
15000
0.65
NS
Vehicle
GC7

h

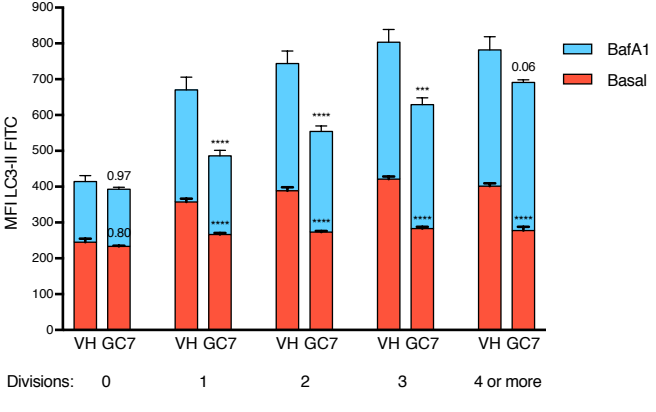
MFI LC3-II FITC
900
800
700
600
500
400
300
200
100
0
0.97
0.80
0.06
****
***
BafA1
Basal
VH GC7
VH GC7
VH GC7
VH GC7
VH GC7
Divisions: 0
1
2
3
4 or more

Figure S1. Related to Figure 1. Spermidine does not affect hematopoiesis in old mice.

(a-i) Various hematopoietic cell types in bone marrow and spleen from young (12 weeks), old (22-24 months), and old mice continuously administered with spermidine in drinking water for 6 weeks as in Fig. 1a were assessed by flow cytometry.

(a/c) Expanded HSCs in bone marrow from old mice. (a) Gating strategy for hematopoietic stem cells (HSCs), multipotent progenitors (MPPs), lymphoid-biased multipotent progenitors (LMPPs), and $Lin^-Sca1^+cKit^+$ cells (LSKs, enriched of hematopoietic stem and progenitor cells) in bone marrow. (c) The abundance of indicated cell types as % of total live cells (left) and their absolute number in tibia and femur of both sides (right). n = 6-7 mice as indicated by dots.

(b/d) Spleen lineages are lymphopenic in old mice. (b) Gating strategy for myeloid cells, B cells, $CD4^+$ T cells, and $CD8^+$ T cells in spleen. (d) The abundance of indicated cell types as % of total live cells (left) and their absolute number in spleen (right). n = 6-17 mice as indicated by dots, combined from 2 independent experiments.

(e/f) Expanded myeloid progenitors in bone marrow from old mice. (e) Gating strategy for megakaryocyte progenitors (MkPs), granulocyte-macrophage progenitors (GMPs), pre-granulocyte/macrophages (Pre-GMs), pre-megakaryocytes/erythrocytes (pre-MegEs), and pro-erythroblast cells (Pro-Erys). (f) The abundance of indicated cell types as % of total live cells (left) and their absolute number in tibia and femur of both sides (right). n = 6-7 mice per group as indicated by dots.

(g-i) Accumulated B cell progenitors in bone marrow from old mice. (g/h) Gating strategy for Hardy fractions A, B, C, D, E, and F (g), and their correlation with B cell developmental stages (h). CLP, common lymphoid progenitors; Pro-B, progenitor B cells; Pre-B, precursor B cells; NF, newly formed B cells; FO, follicular B cells (mature B cells). (i) The abundance of indicated cell types as % of total live cells (left) and their absolute number in tibia and femur of both sides (right). n = 7-11 mice as indicated by dots, pooled from 2 independent experiments. Student's t-test (b/d/f/i).

(j/k) Confirmation of reduced ATG7 expression and autophagy in B cells purified from B cell-specific *Atg7*-knockout mice. (j) B cells were purified from *Mb1-Cre-*, $Atg7^{flox/flox}$ (+/+) and *Mb1-Cre+*, $Atg7^{flox/flox}$ (-/-) mice and the expression of ATG7 was assessed by Western blot (left). For quantification (right), the ATG7 band intensity was normalized to GAPDH first and then to the average of +/+. n = 6 mice. One-tailed Student's t-test. (k) Purified B cells in J were cultured with 10 nM BafA1 or vehicle for 2 h for LC3-II measurement by Western blot (left). For quantification (right), the LC3-II bands intensity was normalized to GAPDH first and then to the average of

Vehicle +/+. n = 4 mice. Paired one-tailed Student's t-test.

(l) Spermidine does not improve IgG1 responses in young mice. Young adult mice were immunized and boosted with NP-CGG. Spermidine administration and serum NP-specific IgG1 measurement were processed as in Fig. 1e. n = 11 (D7), 19 (D14), 12 (D28), 9 (D37), 15 (D51) and 6 (D58) mice, combined from 3 independent experiments. Student's t-test.

Data represented as mean ± SEM. *P≤0.05, **P≤0.01, ***P≤0.001, ****P≤0.0001.

Figure S2. Related to Figure 2. Spermidine does not directly inhibit HAT activities and high-dose spermidine induces cellular stress in Jurkat cells.

(a/b) Spermidine induces autophagy *in vitro*. Jurkat cells were treated with spermidine (Spd) as indicated for 6 h. Autophagy was assessed by LC3-II Western blot (a, n = 5, one-way ANOVA with post hoc Dunnett's test comparing with 0 μM). Autophagosome/autolysosome-specific staining of CytoID was measured by flow cytometry (b, n = 4, Student's t-test).

(c-f) Spermidine does not inhibit HAT activity in Jurkat cells. (c) Jurkat nuclear extract was prepared using the Nuclear/Cytosol Fractionation Kit, incubated with spermidine of indicated concentrations (starting from 0h) and the relative HAT activity was measured using the HAT Activity Colorimetric Assay Kit. n = 3. (d) Jurkat cells were treated with 100 μM spermidine for 6h or 24h. *ATG7* mRNA was measured by quantitative PCR (qPCR) with *GAPDH* used as the reference gene. n = 3. One-way ANOVA with post hoc Dunnett's test comparing with 0 h. (e/f) Jurkat cells were treated with spermidine for 6h and cellular proteins with acetylated lysine residues were pulled down (IP: AcK) and assessed for H3 and ATG7 acetylation (e). To assess ATG7 acetylation in an alternative way, ATG7 was pulled down (IP: ATG7) and acetylation measured with an antibody against AcK (f).

(g) Spermidine does not affect AMPK activity. Jurkat cells were treated with spermidine of indicated concentrations for 6h. AMPK activity was assessed by AMPKα phosphorylation. Cells were treated with 10 μM etoposide for 6h as the positive control. Representative of 3 independent repeats.

(h-m) High-dose spermidine induces cellular stress. (h) Schematic overview of the ER stress PERK- eIF2α-ATF4-CHOP pathway. ER stress activates the protein kinase R-like endoplasmic reticulum kinase (PERK), which phosphorylates eIF2α. Phosphorylated eIF2α facilitates the translation of the transcription factor ATF4, which then induces the expression of CHOP. ATF4 and CHOP induce the expression of multiple stress-response genes including chaperones, apoptosis, and autophagy. (i/j) Jurkat cells were treated with spermidine of indicated concentrations for 6h. The expression of ER stress markers ATF4 (i) and phosphorylation of eIF2α (j) were assessed by Western blot. Representative of 3 independent repeats. (k) Jurkat cells were treated with 100 μM spermidine for 6 h or 24 h. The expression of the ER stress marker *CHOP* was assessed by qPCR with *GAPDH* as the reference gene. n = 3. One-way ANOVA with post hoc Dunnett's test comparing with Vehicle. (l/m) Jurkat cells were treated with spermidine of indicated concentrations for 6 h or 24 h. Cell viability and apoptosis were assessed by Live-Dead (LD) and Annexin V flow cytometry staining. n = 3. Two-way ANOVA with post hoc Dunnett's test comparing with 0 μM.

Data represented as mean ± SEM. *P≤0.05, **P≤0.01, ****P≤0.0001.

Figure S3. Related to Figure 2. Inhibition of eIF5A hypusination reduces autophagy.

(a) *Odc* knockdown efficiency test. NIH 3T3 cells were transfected with non-target siRNA (*siCtrl*) or siRNA targeting two different regions of *Odc* mRNA (*siOdc*-1/2) for 3 days. The expression of *Odc* was assessed by qPCR with *Gapdh* as the reference gene (normalized to *siCtrl*). n = 4. NT, non-treatment. *siOdc-1* was used in all other figures unless specified otherwise.

(b) Spermidine depletion by *siOdc* or DFMO treatment. NIH 3T3 cells were transfected with *siOdc* for 3 days as in Fig. 2b or treated with the ODC inhibitor DFMO (1 mM) for 1 day to deplete cellular spermidine. 10 μM Spermidine was added during the depletion where indicated. Cellular spermidine levels were measured by GC-MS and normalized to total proteins first and then the average of *siCtrl*. n = 3.

(c) NIH 3T3 cells were transfected with *siCtrl*, *siOdc*-1, or *siOdc*-2 for 3 days or treated with DFMO for 24 h. LC3-II was measured by Western blot (left) and quantified (right, n = 5). The LC3-II bands intensity was normalized to GAPDH and then to the average of *siCtrl*.

(d) NIH 3T3 cells were transfected with *siCtrl* or *siOdc* and treated with 10 μM spermidine for 3 days where indicated. LC3-II was measured by Western blot (left) and quantified (right, n = 3).

(e) Quantification of Fig. 2c. The LC3-II bands intensity was normalized to GAPDH first and then to the average of *siCtrl*. n = 3.

(f) Quantification of Fig. 2d. The eIF5A or LC3-II band intensity was normalized to GAPDH first and then to D0. n = 3-6.

(g) NIH 3T3 cells were transfected with *siCtrl* or siRNA targeting two different regions of *Eif5a* mRNA (*siEif5a*-1/2) for 3 days. The expression of LC3-II and eIF5A was measured by Western blot.

(h/i) Inducible knockout of *Dohh* in 3T3 cells reduces eIF5A hypusination and autophagy. (h) The expression of *Dohh* on indicated days post 4-OHT induced deletion was assessed by qPCR. *Gapdh* was used as the reference gene. n = 4. (i) Quantification of Fig. 2e. Left panel: Hypusine (Hyp) was normalized to eIF5A first and then to the average of D0. Right panel: LC3-II was normalized to GAPDH first and then to D0. n = 3-6.

(j) NIH 3T3 cells were transfected with *siCtrl* or siRNA targeting two different regions of *Dhs*

mRNA (*siDhs*-1/2) for 3 days or treated with 10 μM GC7 for 24 h. LC3-II was measured by Western blot (left) and quantified (right, n = 4). *siDhs-1* was used in all other figures unless specified otherwise.

(k) Quantification of Fig. 2f. The LC3-II band intensity was normalized to GAPDH first and then to the average of Vehicle. n = 3.

(l) Spermidine-depleted NIH 3T3 cells by DFMO were rescued with spermidine alone or spermidine together with GC for 24 h. eIF5A hypusination and LC3-II were measured by Western blot (left) and quantified (right, n = 3).

(m) Quantification of Fig. 2g. The blue bars refer to BafA1 minus Vehicle. One-way ANOVA with post hoc Dunnett's test was used to compare the LC3-II staining of either Vehicle (red bar alone) or BafA1 treatment (blue bar plus red bar) on indicated days with D0. n = 3 mice.

(n/o) B cell activation induces the expression of hypusinated eIF5A and autophagy. B cells purified from young wild type mice were cultured with LPS as in Fig. 2g and the expression of overall eIF5A, hypusinated eIF5A and LC3-II was measured by Western blot (n) and the quantification is shown in o. Target protein bands intensity was normalized to GAPDH first, and then to D0. n = 7 mice.

(p) Quantification of Fig. 2i. The protein bands intensity of overall eIF5A (left), hypusinated eIF5A (Hyp, middle), and LC3-II (right) was normalized to GAPDH or eIF5A (for Hyp) first and then to 0 μM GC7. n = 6-10.

(q) GC7 inhibits autophagy in an mTOR-independent manner (not via activating mTOR). LPS-activated murine B cells were treated with 10 μM GC7 for 24 h as in Fig. 2i, or with the mTOR inhibitor Torin 1 for 2 h. The expression of S6 and its phosphorylation (Ser235/236) downstream of mTOR were assessed by Western blot. Representative of 5 independent repeats.

BafA1 was added 2 h before harvest where indicated for autophagy measurement. Data represented as mean ± SEM. One-way ANOVA with post hoc Dunnett's test comparing with *siCtrl* (a/c/j), D0 (o) or 0 μM GC7 (p), or with post hoc Tukey's test (b/d/e/k/l). Two-way ANOVA with post hoc Sidak's test (f/i) or Dunnett's test (h). *P≤0.05, **P≤0.01, ***P≤0.001, ****P≤0.0001, ns, not significant.

Figure S4. Related to Figure 3. eIF5A and its hypusination are required for TFEB expression.

(a) An aliquot of protein samples for MS in Fig. 3a was assessed by Western blot for cell fractionation efficiency. W: whole cell lysate; N: nuclear fraction; C: cytoplasmic fraction.

(b) Gating strategy for the FACS sorting in Fig. 3b. Live B cells ($CD19^+$) that divided four times or more were collected.

(c) Quantification of Fig. 3f. n = 3.

(d) NIH 3T3 cells were transfected with *siEif5a*-1/2 for 3 days. TFEB expression was measured by Western blot (left) and quantified (right, n = 3).

(e) Quantification of Fig. 3g. n = 4.

(f) NIH 3T3 cells were transfected with *siOdc*-1/2 for 3 days or treated with 1 mM DFMO for 24 h. TFEB expression was measured by Western blot (left) and quantified (right, n = 3).

(g) *siOdc*-transfected NIH 3T3 cells were treated with 10 μM spermidine and transfected with *siEif5a*. TFEB expression was analyzed by Western blot (left) and quantified (right, n = 3).

(h) NIH 3T3 cells were depleted from spermidine by 1 mM DFMO and rescued with spermidine alone or spermidine together with 10 μM GC7 for 24 h. TFEB was measured by Western blot (left) and quantified (right, n = 3).

TFEB expression was quantified by normalizing to GAPDH first and then to the average of *siCtrl* (c-h). n = 3 (c-e/f-h) or 4 (e). One-way ANOVA with post hoc Dunnett's test comparing with *siCtrl* (c/d/f) or Tukey's test (e/g/h).

Figure S5. Related to Figure 4. Spermidine maintains protein synthesis.

(a) Jurkat T cells were cultured with 1 mM DFMO together with or without 10 μM spermidine. Protein translation rate was determined by OPP-Click assay. n = 3-4. One-way ANOVA with post hoc Tukey's test. ****P≤0.0001.

Figure S6. Related to Figure 5. Hypusinated eIF5A is essential for hematopoiesis and B cell activation.

(a/b) Gating strategy for transitional (T) B cells, follicular (FO) B cells, marginal zone (MZ) B cells and the contribution of $CD45.2^+$ fraction in peripheral blood (a) and spleen (b).

(c) The contribution of $CD45.2^+$ cells to spleen myeloid cells ($CD11b^+Gr1^+$) of *Dhs* chimera mice in Fig. 5a. n = 5-7 mice as indicated by dots. Welch's t-test.

(d/e) *Dhs* deletion efficiency was tested by PCR. The wild type *Dhs*, floxed *Dhs*, and tamoxifen-induced deletion of *Dhs* were assessed by genotyping DNA extracted from pooled peripheral blood of the chimeric mice on day 8 post tamoxifen administration (d) or from bone marrow and spleen on day 34 post tamoxifen administration (e). 4-OHT-induced *Dhs* deletion (D0/D5) in 3T3 cells derived from CAG-Cre/$Esr1^+$, $Dhs^{f/f}$ mouse embryonic fibroblasts was used as positive control.

(f) The cellularity of bone marrow (tibia and femur of both sides) (left) and spleen (right) of WT and KO *Dhs* chimera mice in Fig. 5a. n = 5-7 mice as indicated by dots. Student's t-test.

(g) Quantification of Fig. 5f. n = 3 mice. Student's t-test.

(h) Quantification of Fig. 5h. Autophagy levels of B cells after the indicated number of divisions was measured by LC3-II flow cytometry. Blue bars refer to the geometric mean fluorescence intensity (MFI) of BafA1 minus Basal LC3-II. Two-way ANOVA with post hoc Sidak's test was used to compare the LC3-II levels of either Basal (red bar alone) or BafA1 treatment (blue bar plus red bar) between Vehicle (VH) and GC7-treated cells within each group. n = 3 mice. ***P≤0.001, ****P≤0.0001.

Materials and Methods

KEY RESOURCES TABLE

REAGENT	SOURCE	IDENTIFIER
Antibodies (Ghada for human)		
GAPDH	Millipore	MAB374, RRID:AB_2107445
LC3	Sigma	L8918, RRID:AB_1079382
eIF5A	BD Biosciences	611976, RRID:AB_399397
Hypusine	Millipore	ABS1064, RRID:AB_2631138
ATG7	Abcam	Ab133528, RRID:AB_2532126
H3	Cell Signaling	9715, RRID:AB_331563
S6	Cell Signaling	2317, RRID:AB_2238583
pS6 (Ser235/236)	Cell Signaling	4858, RRID:AB_916156
AMPKα	Cell Signaling	2793, RRID:AB_915794
pAMPKα (T172)	Cell Signaling	2535, RRID:AB_331250
AcK	Cell Signaling	9441, RRID:AB_331805
ATF4	Santa Cruz	sc-200, RRID:AB_2630429
eIF2α	Cell Signaling	2103, RRID:AB_836874
p-eIF2α (Ser51)	Cell Signaling	9721, RRID:AB_330951
TFEB	Bethyl	A303-673A, RID:AB_11204751
DHS	Abcam	Ab190266
β-Actin	Cell Signaling	3700, RRID:AB_2242334
IRDye 800CW Donkey Anti-Rabbit IgG (H+L)	LI-COR	926-32213, RRID:AB_621848
IRDye 680RD Donkey Anti-Mouse IgG (H+L)	LI-COR	926-68022, RRID:AB_10715072
CD16/CD32 Monoclonal Antibody (FcR Block)	Thermo Fisher	14-0161-85, RRID:AB_467134
Pacific Blue™ anti-mouse/human CD44 Antibody	BioLegend	103020, RRID:AB_493683
Pacific Blue™ anti-mouse TER-119/Erythroid Cells Antibody	BioLegend	116232, RRID:AB_2251160
Pacific Blue™ anti-mouse CD45.1 Antibody	BioLegend	110722, RRID:AB_492866
Pacific Blue™ anti-mouse Ly-6G/Ly-6C (Gr-1) Antibody	BioLegend	108430, RRID:AB_893556
Pacific Blue™ anti-mouse Ly-6A/E (Sca-1) Antibody	BioLegend	122520, RRID:AB_2143237
Brilliant Violet 605™ anti-mouse CD41 Antibody	BioLegend	133921, RRID:AB_2563933
Brilliant Violet 605™ anti-mouse CD4 Antibody	BioLegend	100451, RRID:AB_2564591
Brilliant Violet 605™ anti-mouse/human CD45R/B220 Antibody	BioLegend	103244, RRID:AB_2563312
Ly-6A/E (Sca-1) Monoclonal Antibody, PerCP-Cyanine5.5	Thermo Fisher	45-5981-82, RRID:AB_914372
CD19 Monoclonal Antibody, PerCP-Cyanine5.5	Thermo Fisher	45-0193-82, RRID:AB_1106999
FITC anti-mouse Ly-6A/E (Sca-1) Antibody	BioLegend	108106, RRID:AB_313343
CD43 Monoclonal Antibody, FITC	Thermo Fisher	11-0431-81, RRID:AB_465039
FITC anti-mouse CD4 Antibody	BioLegend	100406, RRID:AB_312691
FITC anti-mouse IgM Antibody	BioLegend	406506, RRID:AB_315056
PE anti-mouse/human CD45R/B220 Antibody	BioLegend	103208, RRID:AB_312993
PE anti-mouse Ly-51 Antibody	BioLegend	108308, RRID:AB_313365
PE anti-mouse/human CD44 Antibody	BioLegend	103008, RRID:AB_312959
PE anti-mouse Ly-6G/Ly-6C (Gr-1) Antibody	BioLegend	108408, RRID:AB_313373
PE anti-mouse CD135 Antibody	BioLegend	135306, RRID:AB_1877217
PE anti-mouse CD19 Antibody	BioLegend	115508, RRID:AB_313643
PE anti-mouse/human CD11b Antibody	BioLegend	101208, RRID:AB_312791
CD4 Monoclonal Antibody (GK1.5), PE-Cyanine5	Thermo Fisher	15-0041-82, RRID:AB_468695
PE/Cy5 anti-mouse CD5 Antibody	BioLegend	100610, RRID:AB_312739
PE/Cy5 anti-mouse CD8a Antibody	BioLegend	100710, RRID:AB_312749
PE/Cy5 anti-mouse/human CD11b Antibody	BioLegend	101210, RRID:AB_312793
PE/Cy5 anti-mouse CD11c Antibody	BioLegend	117316, RRID:AB_493566
PE/Cy5 anti-mouse/human CD45R/B220 Antibody	BioLegend	103210, RRID:AB_312995
PE/Cy5 anti-mouse CD3ε Antibody	BioLegend	100310, RRID:AB_312675
TCR beta Monoclonal Antibody, PE	Thermo Fisher	12-5961-82, RRID:AB_466066

TCR gamma/delta Monoclonal Antibody, PE-Cyanine5	Thermo Fisher	15-5711-82, RRID:AB_468804
PE/Cy5 anti-mouse TER-119/Erythroid Cells Antibody	BioLegend	116210, RRID:AB_313711
PE/Cy5 anti-mouse NK-1.1 Antibody	BioLegend	108716, RRID:AB_493590
PE/Cy5 anti-mouse Ly-6G/Ly-6C (Gr-1) Antibody	BioLegend	108410, RRID:AB_313375
PE/Cy7 anti-mouse CD43 Antibody	BioLegend	143210, RRID:AB_2564349
PE/Cy7 anti-mouse CD8a Antibody	BioLegend	100722, RRID:AB_312761
PE/Cy7 anti-mouse CD19 Antibody	BioLegend	115520, RRID:AB_313655
PE/Cy7 anti-mouse IgM Antibody	BioLegend	406514, RRID:AB_10642031
PE/Cy7 anti-mouse CD150 (SLAM) Antibody	BioLegend	115914, RRID:AB_439797
APC anti-mouse CD105 Antibody	BioLegend	120414, RRID:AB_2277914
APC anti-mouse CD3ε Antibody	BioLegend	100312, RRID:AB_312677
TCR beta Monoclonal Antibody, APC	Thermo Fisher	17-5961-81, RRID:AB_469480
TCR gamma/delta Monoclonal Antibody, APC	Thermo Fisher	17-5711-82, RRID:AB_842756
APC anti-mouse NK-1.1 Antibody	BioLegend	108710, RRID:AB_313397
APC anti-mouse/human CD45R/B220 Antibody	BioLegend	103212, RRID:AB_312997
APC anti-mouse/human CD11b Antibody	BioLegend	101212, RRID:AB_312795
APC anti-mouse Ly-6G/Ly-6C (Gr-1) Antibody	BioLegend	108412, RRID:AB_313377
APC anti-mouse CD24 Antibody	BioLegend	138506, RRID:AB_2565651
APC anti-mouse CD4 Antibody	BioLegend	100412, RRID:AB_312697
APC anti-mouse CD48 Antibody	BioLegend	103412, RRID:AB_571997
APC anti-human CD19	BioLegend	302212, RRID:AB_314242
Alexa Fluor® 700 anti-mouse CD45.2 Antibody	BioLegend	109822, RRID:AB_493731
Alexa Fluor® 700 anti-mouse CD8a Antibody	BioLegend	100730, RRID:AB_493703
CD8a Monoclonal Antibody, APC-eFluor 780	Thermo Fisher	47-0081-82
APC/Cy7 anti-mouse/human CD11b Antibody	BioLegend	101226, RRID:AB_830642
APC/Cy7 anti-mouse IgD Antibody	BioLegend	405716, RRID:AB_10662544
APC/Cy7 anti-mouse CD19 Antibody	BioLegend	115530, RRID:AB_830707
CD117 (c-Kit) Monoclonal Antibody (2B8), APC-eFluor 780	Thermo Fisher	47-1171-82, RRID:AB_1272177
Goat Anti-Mouse IgG1, Human ads-AP	SouthernBiotech	1070-04
Rabbit IgG (IP)	Santa Cruz	sc-2027, RRID:AB_737197
ATG7 (IP)	Abcam	Ab58735, RRID:AB_940290
AcK (IP)	Cell Signaling	9441, RRID:AB_331805
siRNA		
Eif5a #1	Dharmacon	D-057410-02
Eif5a #2	Dharmacon	D-057410-04
Odc #1	Dharmacon	D-041731-03
Odc #2	Dharmacon	D-041731-17
Dhs #1	Dharmacon	D-054953-01
Dhs #2	Dharmacon	D-054953-02
Non-target	Dharmacon	D-001220-01
TaqMan® probes		
Gapdh	Thermo Fisher	Mm99999915_g1
Odc1	Thermo Fisher	Mm01964631_g1
Dohh	Thermo Fisher	Mm00505991_m1
Atg9b	Thermo Fisher	Mm01157883_g1
Ctsd	Thermo Fisher	Mm00515586_m1
Gla	Thermo Fisher	Mm00516323_m1
Neu1	Thermo Fisher	Mm00456846_m1
Psap	Thermo Fisher	Mm00478338_m1
Tfeb	Thermo Fisher	Mm00448968_m1
Wipi1	Thermo Fisher	Mm00461219_m1
GAPDH	Thermo Fisher	Hs02758991_g1
ATG7	Thermo Fisher	Hs00893770_m1
CHOP	Thermo Fisher	Hs00358796_g1
Cell lines		
Jurkat	ATCC	RRID:CVCL_0367
NIH 3T3	ATCC	RRID:CVCL_0594

HEK293T	ATCC	RRID:CVCL_0063
Deposited data: doi:10.17632/cd4f7j2hbh.1		

Mice

Young (6-12 weeks) and old (22-24 months) C57BL/6J wild type mice (RRID:IMSR_JAX:000664) were purchased from Charles River UK. CD45.1^{+} B6.SJL mice (RRID:IMSR_JAX:100012) were purchased from Charles River UK and bred in BSU at the Kennedy Institute of Rheumatology. *Mb1-cre* mice were a kind gift from M Reth, *Atg7^{flox}* mice from M Komatsu, GFP-LC3 mice from N Mizushima and Stefan Balabanov made the bone marrow from inducible *Dhs^{flox}* mice available [1]. 5 mM Spermidine (CAY14918, Cambridge Bioscience) was administered to mice in the drinking water, changed three times per week. All mice were held at Biomedical Services, University of Oxford. Animal experiments were approved by the local ethical review committee and performed under UK project licenses PPL 30/2809 and then PPL 30/3388.

Bone marrow chimera

Bone marrow cells were collected from the femur and tibia of the donor mice (*Dhs$^{+/+}$ or Dhs$^{-/-}$* CD45.2^{+}, with young B6.SJL CD45.1^{+} mice as competitors) and frozen in cryopreservation medium for long-term storage. Carefully thawed cells were counted and mixed at the indicated ratio for intravenous (iv) injection. The recipient B6.SJL mice were lethally irradiated (450 cGy twice, 4 hours apart) and rested for 1 hour prior to injection. A total of 1.5 million bone marrow cells were injected intravenously into recipient mice. After at least 16 weeks of long-term reconstitution, tamoxifen (Sigma) dissolved in corn oil was administered via oral gavage (5 mg/mouse/day for 5 consecutive days) and peripheral blood and organs were collected for analysis.

Mouse immunization

Mice were injected intraperitoneally (ip) with 50 µg NP-CGG (N-5055D-5, Biosearch Technologies, dissolved in PBS) in Imject Alum adjuvant (Thermo Fisher) on day 0 followed by secondary immunization on or after day 42 (50 µg NP-CGG in PBS ip). Peripheral blood samples were collected from tail vein on indicated days.

Western blot

Cells in suspension were washed with PBS and lysed using NP-40 lysis buffer containing proteinase inhibitors (Sigma) and phosphatase inhibitors (Sigma) on ice. After spinning down the debris, protein concentration in the supernatant was quantified by BCA Assay (23227, Thermo Fisher). Reducing Laemmli Sample Buffer was then added to the supernatant and heated at 100°C for 5 minutes. 5-20 µg proteins were loaded for SDS-PAGE analysis. For LC3 western blot, 15% Tris-HCl gel and SDS running buffer was used to separate LC3-I and LC3-II. For non-LC3 western blot, NuPAGE Novex 4-12% Bis-Tris gradient gel (Thermo Fisher) with MES running buffer (Thermo Fisher) was used. Proteins were transferred to a PVDF membrane (IPFL00010, Millipore) and blocked with 5% skimmed milk-TBST. Membranes were incubated with primary antibodies dissolved in 1% milk overnight and secondary

antibodies dissolved in 1% milk with 0.01% SDS for imaging using the Odyssey CLx Imaging System. Data were analyzed using Image Studio Lite.

Mouse B cell purification and stimulation

RBC-lysed mouse splenocytes were purified using the Pan B Cell Isolation Kit II (130-104-443, Miltenyi). Cells were cultured at a density of 1 million/ml supplemented with 10 μg/ml LPS (Santa Cruz) for stimulation. Medium was replaced on day 3 of culture by replacing half volume with fresh culture medium containing LPS followed by analysis on day 4 and day 5.

NP-IgG1 ELISA

ELISA plates (675061, Greiner Bio-One) were coated with 5 μg/ml NP-BSA (N-5050H-10, Biosearch Technologies) in bicarbonate/carbonate buffer at 4°C overnight. After three washes with PBS, plates were blocked with 5% skimmed milk in PBS at 37°C for 1 hour, followed by 3 x PBS washes. Serum samples diluted in 1% milk were added and incubated at 37°C for 1 hour. For relative quantification, a standard serum sample was made by pooling samples on day 7, post-secondary immunization from a prior experiment, then aliquoted for all subsequent experiments. Serum samples of various days were serially diluted first to determine the proper dilution, and 1:1000-1:5000 was chosen for NP-IgG1 ELISA. After serum sample incubation, plates were washed 6 times with PBS-0.05% Tween 20 followed with detection antibody incubation at 37°C for 1 hour. Alkaline phosphatase- (AP-) conjugated goat-anti mouse IgG1 (Southern Biotech) detection antibody was diluted in 1% milk-PBS at a ratio of 1:2000. After 5 washes with PBS-0.05% Tween 20 and once with PBS, AP-substrate (S0942, Sigma) dissolved in pNPP buffer was added for 15-20 min and absorbance was measured at 405 nm by ELISA plate reader (FLUOstar Omega, BMG Labtech).

ELISpot

MultiScreenHTS-HA filter plates (MSHAS4510) were first rinsed with 35% ethanol for 30 seconds and washed 3 times with PBS. Plates were coated with 20 μg/ml NP-BSA in PBS at 4°C over night. After three washes with PBS, plates were blocked with RPMI-1640 medium supplemented with 10% FBS at 37°C for 30 minutes. Then bone marrow cells were added in duplicates in culture medium at the density of $3x10^5$ /100 μL/ well and cultured at 37°C over night. Plates were then washed 3 times with PBS and 3 times with PBS-0.05% Tween 20. AP-conjugated anti-mouse IgG1 detection antibody diluted in 1% FBS was added to plates for 1 hour incubation at 37°C. After 5 washes with PBS-0.05% Tween 20 and once with PBS, AP substrate (170-6432, Bio-Rad) was added for spot development. Plates with clear spots and clean background were washed with water to stop development, dried, and counted with the AID ELISpot Reader System (ELR078IFL, AID GmbH).

Plasmid construction

The TFEB (polyproline motif)-mCherry, 13P-mCherry and Random-mCherry were cloned into pMSCV–IRES-EGFP. The internal ribosome entry site (IRES) allows the expression of GFP independent of

mCherry. A flexible GSGSG linker was inserted between the targeted sequence and mCherry to assist folding of the fusion protein. The target sequences were inserted by HindIII and BamHI.
Targeted sequences: TFEB: (M)HFQSPPPVPGEVL; 13P: (M)PPPPPPPPPPPPP; Random: (M)AGYRLIDNWKVSH.

Cell drug treatments

10-100 μM GC7 (Millipore) was added for 24 hours to B cells on day 2 after B cell stimulation (unless otherwise indicated) or to Jurkat cells. 10 nM bafilomycin A1 (Cayman Chemical), 10 μg/ml cycloheximide (Sigma), or 100 nM Torin 1 (Cayman Chemical) were added to cells for 2 hours. 10 μM etoposide (Cayman Chemical) was added to cell culture for 6 hours, or 1 mM difluoromethylornithine (DFMO, Enzo Life Sciences) for 24 hours.

Cell culture systems

Cells (Jurkat , NIH 3T3, HEK293T) were cultured in RPMI-1640 medium supplemented with 10% FBS, Penicillin-Streptomycin (P/S), and L-Glutamine (all Sigma) in 5% CO_2 at 37°C. The IPTG-inducible MISSION shRNA lentiviral vector pLKO-puro-IPTG-3xLacO contains shRNA against the 3'-UTR of murine eIF5A mRNA (custom-made from #SHCLND-NM181582-TRCN0000125229, Sigma) or a corresponding non-target shRNA control (#SHC332-1EA, Sigma). 100 μM IPTG (Thermo Fisher) was used to induce the expression of shRNA. Stable transduction of the lentivirus was performed as previously described [2]. Immortalized *Dohh*$^{flox/flox}$ and *Dohh*$^{+/+}$ 3T3 cells were established from mouse embryonic fibroblasts [3]. 100 nM 4-OHT (H6278, Sigma) was used to induce the knockout of *Dohh*. NIH 3T3 cells were transfected with siRNA according to Thermo Fisher protocol (13778075, Lipofectamine® RNAiMAX Reagent). Cells were collected on day 3 post-transfection for western blot analysis. For plasmid transfection assay, NIH 3T3 cells pretreated with 10 μM GC7 for 24 hours were transfected with the indicated plasmids using Lipofectamine 3000 according to the manufacturer's protocol. mCherry and GFP expression was quantified by flow cytometry 24 hours post transfection.

Flow cytometry

Cells were stained with fixable Zombie Aqua Live/Dead staining (423102, Biolegend), FcR block, followed by surface marker antibodies and analyzed with four-laser LSR Fortessa X-20. Acquired data were analyzed using FlowJo 10.2. For LC3-II flow cytometry (FACS) staining, the FlowCellect™ Autophagy LC3 antibody-based assay kit (FCCH100171, Millipore) and for CellTrace staining, CellTrace Violet (C34557, Thermo Fisher) were used according to the manufacturer's protocol.

CytoID staining

Cells were stained with CytoID (ENZ-51031-K200, Enzo Life Sciences) according to manufacturer's protocol. Briefly, cells were re-suspended in CytoID staining solution (1:4000 diluted in RPMI without phenol red (R1780, Sigma) supplemented with 5% FBS) and incubated at 37°C for 30 minutes in the dark. Then cells were washed once, followed by surface marker staining and FACS analysis without fixation.

Immunoprecipitation

After various treatments an equal number of cells were collected, washed with PBS and lysed using NP-40 lysis buffer with proteinase and phosphatase inhibitors on a rotator at 4°C for 20 minutes., 950 µL lysis buffer was used for 25 million Jurkat cells. Cell debris was centrifuged down at 13000 rpm for 15 minutes at 4°C. 50 µL supernatant was collected as whole cell lysate (input control), and the protein concentration was measured by BCA assay. The remaining supernatant was mixed with 15 µL Protein A Agarose beads (Thermo Fisher) in PBS, then rotated at 4°C for 15 minutes to pre-clear the lysate. The beads were removed by centrifugation at 6000 rpm for 1 minute. Immunoprecipitation (IP) antibody (AcK, ATG7, or rabbit IgG) and 20 µL Protein A agarose beads were added to the lysate and then rotated at 4°C overnight. The beads were washed twice with NP-40 lysis buffer containing proteinase and phosphatase inhibitors and the supernatant discarded. 35 µL 2X Reducing Laemmli Sample Buffer was added to the beads and heated at 100°C for 5 minutes.and supernatant used for Western blot analysis.

Quantitative PCR

RNA was extracted using the RNeasy Plus Mini Kit (74134, Qiagen). The concentration of RNA was measured using NanoDrop1000 (Thermo Fisher), followed by reverse transcription using the High Capacity RNA-to-cDNA Kit (4387406, Thermo Fisher). Taqman probes (Thermo Fisher), TaqMan Gene Expression Master Mix (4369016, Thermo Fisher), and the ViiA 7 Real-Time PCR System (Thermo Fisher) were used for quantitative PCR. ΔΔCt method was used for the quantification of target mRNAs expression using *Gapdh* as the reference gene.

Confocal microscopy

B cells from GFP-LC3 mice were MACS-purified and fixed with 4% paraformaldehyde at room temperature for 10 min. After nuclear staining with DAPI (Sigma), cells were transferred to slides using Cytospin 3 cytocentrifuge (Shandon) and imaged with the Olympus FV1200 Laser Scanning Microscope. CellProfiler software was used for automatic autophagosome quantification. Nuclei were defined in DAPI channel (diameter of 45-100 pixel units), autophagosomes were defined in GFP channel (diameter of 3-15 pixel units,1 pixel unit =100 nm). A threshold of 1-10 cellular GFP spots was used for analysis.

Cell fractionation

Cells in a 1.5 mL Eppendorf tube were washed once with cold PBS and re-suspended in HLB buffer (10 mM Tris-HCl pH 7.5, 10 mM NaCl, 2.5 mM MgCl2) with protease inhibitors and phosphatase inhibitors, then HLB+2N buffer (HLB+0.4% NP-40, 1N is 0.2% NP-40) was added and carefully mixed. Samples were incubated on ice for 5 minutes and then underlayed with 200 uL HLB+NS buffer (HLB+0.2% NP-40+10% sucrose). Samples were centrifuged at 500 g for 5 minutes and the upper half of the supernatant was collected as the cytoplasmic fraction. The remaining liquid was discarded and the nuclear pellet was washed once more with HLB buffer and lysed with NP-40 lysis buffer. All procedures were performed on ice.

Proteomics mass spectrometry

LPS-stimulated mouse B cells were treated with 10 μM GC7 on day 2 for 24 hours. Cells were collected and fractionated for label-free quantitative mass spectrometry (MS) analysis. For SILAC MS, B cells stained with CellTrace Violet (C34557, Thermo Fisher) were cultured in two types of medium: light and heavy. In light medium, SILAC RPMI-1640 medium (89984, Thermo Fisher) supplemented with 1.15 mM L-Arg (Sigma) and 0.22 mM L-Lys (Sigma), 10% dialysed FBS (Sigma), and P/S, L-Glutamine, 50 μM 2-mercaptoethanol, 20 mM HEPES were used. In heavy medium, $^{13}C_6{}^{15}N_4$-L-Arg (Arg-10, Silantes) and $^{13}C_6{}^{15}N_2$-L-Lys (Lys-8, Silantes) were used instead of the light arginine and lysine respectively. 10 μM GC7 was added to either light or heavy medium in two repeats. After GC7 treatment, dead cells were firstly removed using the Dead Cell Removal Kit (Miltenyi). An identical number of cells that had divided at least 4 times in light or heavy medium were collected by FACS, and mixed for cell fractionation and protein MS analysis.

Peptide samples were prepared using the Filter Aided Sample Preparation (FASP), as previously described [4]. Briefly, Vivacon 500 filters (Sartorius, VN01H02 10 kDa/VNCT01) were pre-washed with 200 μL 0.1% trifluoroacetic acid in 50% acetone. Lysate samples were loaded to the filter and denatured with 200 μL 8 M urea in 100 mM triethylammonium bicarbonate buffer (TEAB) for 30 minutes at room temperature. Denatured proteins were reduced by 10 mM tris (2-carboxyethyl) phosphine (TCEP) for 30 minutes at room temperature and alkylated with 50 mM chloroacetamide for 30 minutes at room temperature in the dark. Subsequently, 1 μg LysC (Wako) in 150 μL 50 mM TEAB containing 6M urea was added and incubated at 37°C for 4 hours. Then the buffer was diluted to 2 M urea by 50 mM TEAB, followed by adding 0.5 μg trypsin (Promega) overnight at 37°C. Trypsinised samples were centrifuged and the flow-through, containing peptides, was dried and resuspended in 70 μL 10% formic acid (or 5% formic acid and 5% DMSO for SILAC experiment).

Peptides were separated on an Ultimate 3000 UHPLC system (Thermo Fisher) and electrosprayed directly into a QExactive mass spectrometer (Thermo Fisher) The peptides were trapped on a C18 PepMap100 pre-column (300 μm i.d. x 5 mm, 100 Å, Thermo Fisher) using solvent A (0.1% formic acid in water) at a pressure of 500 bar, then separated on an in-house packed analytical column (75 μm i.d. packed with ReproSil-Pur 120 C18-AQ, 1.9 μm, 120 Å, Dr. Maisch GmbH) using a linear gradient (length: 120 minutes, 15% to 35% solvent B (0.1% formic acid in acetonitrile), flow rate: 200 nl/min). Data were acquired in a data-dependent mode (DDA). Full scan MS spectra were acquired in the Orbitrap (scan range 350-1500 m/z, resolution 70000, AGC target 3e6, maximum injection time 50 ms). The 10 most intense peaks were selected for HCD fragmentation at 30% of normalised collision energy at resolution 17500, AGC target 5e4, maximum injection time 120 ms with first fixed mass at 180 *m/z*. Charge exclusion was selected for unassigned and 1+ ions. The dynamic exclusion was set to 20 seconds.

Raw MS data were processed by MaxQuant (version 1.5.0.35i) for peak detection and quantification [5, 6]. MS spectra were searched against the *Mus musculus* UniProt Reference proteome (retrieved 12/01/17) alongside a list of common contaminants, using the Andromeda search engine with the following search parameters: full tryptic specificity, allowing two missed cleavage sites, fixed modification was set to

carbamidomethyl (C) and the variable modification to acetylation (protein N-terminus) and oxidation (M). The search results were filtered to a false discovery rate (FDR) of 0.01 for proteins, peptides and peptide-spectrum matches (PSM). Protein intensity distributions were log2 transformed and median-centred using Perseus (version 1.5.5.3). For the SILAC analysis, missing values were replaced by an estimated background noise value. Proteins without greater-than-background values in both replicates for at least one condition were removed. MA plots were generated using R (version 3.4.2). Reviewed autophagy proteins were searched against the *Mus musculus* UniProt database. Data from the independently analyzed cytoplasmic and nuclear proteins were shown as overlaid MA-plots wherein the log2 average (GC7 + Vehicle) intensity (A) is plotted on *x* versus the log2 (GC7:Vehicle) fold change (M) plotted on *y*.

Spermidine measurement by gas chromatography mass spectrometry (GC-MS)

Cells were washed with PBS and the pellet resuspended in lysis buffer (80% methanol + 5% Trifluoroacetic acid) spiked with 2.5 µM 1,7-diaminoheptane (Sigma). The cell suspension, together with acid-washed glass beads (G8772, Sigma), was transferred to a bead beater tube and homogenized in a bead beater (Precellys 24, Bertin Technologies) for four cycles (6500 Hz, 45 s) with 1 minute of ice incubation between each cycle. The homogenized samples were centrifuged at 13,000 g for 20 minutes at 4°C. The supernatant was collected and dried overnight. For chemical derivatization, 200 µL trifluoroacetic anhydride was added to the dried pellet and incubated at 60°C for 1 hour, shaking at 1200 rpm. The derivatization product was dried, re-suspended in 30 µL isopropanol and transferred to glass loading-vials. The samples were analyzed using a GCxGC-MS system as described [7]. The following parameters were used for quantification of the 1D-GC-qMS data: Slope: 1000/min, width: 0.04 s, drift 0/min and T. DBL: 1000 min without any smoothing methods used.

OPP-Click Assay

Protein synthesis rate was measured using the Click-iT Plus OPP Protein Synthesis Assay (C10456, Thermo Fisher) according to manufacturer's protocol. Geometric mean fluorescence intensity (normalized to vehicle) was used as an indicator of the relative protein translation rate.

Ribosome profiling

The sequencing library was prepared according to the reference [8, 9] with the following changes. LPS-activated B cells were MACS-purified with the Dead Cell Removal Kit (Miltenyi) to remove dead cells prior to cell lysis. 100 µg/ml cycloheximide was used in the lysis buffer. The B cell lysate was spiked with the *S. cerevisiae* lysate at the ratio of 13 million B cells: 270 million yeast cells (which equals to 20:4 µg miRNA). Clarified B cell and yeast lysates were RNase I-digested, ribosome purified and miRNA extracted to determine the miRNA yield for spiking. Size exclusion chromatography (27-5140-01, GE Healthcare) was used to recover ribosomes. The miRNeasy Micro Kit (Qiagen) was used to purify miRNAs. The Ribo-Zero Gold rRNA Removal Kits (illumina, MRZG126, MRZY1306) were used to deplete ribosomal RNAs, in which the Ribo-Zero Removal Solutions from the mouse and yeast kits were mixed at the ratio of 8 µL : 4 µL to remove both mouse and yeast rRNAs. The following barcoding primers were used for next generation sequencing. 1. 5′-

AATGATACGGCGACCACCGAGATCTACAC GATCGGAAGAGCACACGTCTGAACTCCAGTCA CATGCCATCCGACGATCATTGATGG. 2. 5′-AATGATACGGCGACCACCGAGATCTACAC GATCGGAAGAGCACACGTCTGAACTCCAGTCA CTGCATCTCCGACGATCATTGATGG. The libraries were sequenced at the Biopolymers Facility, Harvard Medical School.

For the purposes of alignment, the reference genome assemblies for Mus musculus (GRCM38) and Saccharomyces cerevisiae (SacCer3) were concatenated to create a combined genome fasta file. A combined rRNA transcript file was also created using the sequences listed in Table S1. Prior to alignment, Adaptor sequence (ATCTCGTATGCCGTCTTCTGCTTG) was removed from demultiplexed reads and low quality reads (Phred score < 20) were discarded. To remove contaminating rDNA reads, reads were aligned to the combined rDNA genome using bowtie2 and all unaligned reads were kept for alignment to the combined genome. Non-rDNA reads were aligned to the combined genome using bowtie2 and the following parameters: -t -N 1 and uniquely aligning reads were extracted using samtools view -bq 10. All post-alignment analysis was performed using custom scripts written in R. P-site offsets for each read-length from 26 to 35 nts in the rpf libraries were determined by generating metagenes relative to the START codon and applied to aligned reads (Table S2). For all metagenes, transcripts with no reads within the window of interest were excluded from analysis before applying any other filters. Additionally, for each position in the windows of the 5' and 3' metagenes, the highest and lowest 0.1% of signals were removed from analysis.

The 100 most stalled PPP motifs were identified using the "stall-ratio" defined as the ratio of coverage over position +3 relative to the first proline against the mean coverage of the entire 80 bp window. The following filters were also applied to exclude windows with only a few sporadic spikes which may not reflect real translation. To be considered, a window must contain > 10 reads outside of the +3 position and the window must have reads in at least 5 positions. After applying these filters, the 100 genes with the highest stall-ratios were selected for metagenes.

Human B cell assays

Peripheral blood mononuclear cells (PBMCs) were isolated from blood of healthy donors using Ficoll-Paque. The study was approved by the Ethics Committee of Oxford University. B cells were then sorted using a negative selection kit (B Cell Isolation Kit II, human, Miltenyi Biotec) according to the manufacturer's protocol. B cells (5×10^5 cells) were seeded in 24-well plates, then activated with anti-IgM (5 μg/ml, Jackson Immuno Research) and CD40L (100 ng/ml, Enzo Life science) and treated with 1 mM DFMO, 10 μM spermidine, or with both for 7 days. Cells then were lysed for western blotting or stained for LC3 measurement by flow cytometry as previously described. IgG release in culture supernatants was measured by heterologous two-site sandwich ELISA, according to the manufacturer's protocol (Invitrogen).

Statistical analyses

Prism software (GraphPad) was used for statistical analyses. Data are represented as either box-and-whisker plots showing whiskers and outliers by Tukey method or mean ± SEM. All data points refer to the measurement of distinct samples (biological repeats). Paired or unpaired two-tailed Student's t-test was used for comparisons between two normally distributed data sets with equal variances. One-tailed Student's t-test was used when the null hypothesis has a clear direction according to current knowledge (*e.g.* spermidine is an autophagy inducer in multiple systems or Bafilomycin A1 treatment leads to accumulation of LC3-II). Welch's unequal variances t-test was used when the two normally distributed data sets have unequal variances. Holm-Sidak method was used to adjust P values of a family of multiple t-tests with a single null hypothesis. Paired or unpaired one/two-way ANOVA, followed with post hoc Sidak's test (comparing two means within each group), Dunnett's test (comparing multiple means with the single control within each group), or Tukey's test (comparing the mean of each sample with the mean of every other sample), was used for multiple comparisons of normally distributed datasets with one/two variables. Mann-Whitney U test was used for comparisons between non-parametric datasets. Linear regression with 95% confidence interval was used to assess the relationships between age and the expression of target proteins or spermidine levels, in which R^2 was used to assess the goodness of fit and the P value calculated from F test was used to assess if the slope was significantly non-zero. P value was used to quantify the statistical significance of the null hypothesis testing. *P≤0.05, **P≤0.01, ***P≤0.001, ****P≤0.0001, ns, not significant.

References

1. Pallmann, N. *et al.* Biological Relevance and Therapeutic Potential of the Hypusine Modification System. *The Journal of biological chemistry* (2015).
2. Preukschas, M. *et al.* Expression of eukaryotic initiation factor 5A and hypusine forming enzymes in glioblastoma patient samples: implications for new targeted therapies. *PloS one* **7**, e43468 (2012).
3. Sievert, H. *et al.* A novel mouse model for inhibition of DOHH-mediated hypusine modification reveals a crucial function in embryonic development, proliferation and oncogenic transformation. *Disease models & mechanisms* **7**, 963-976 (2014).
4. Wisniewski, J.R., Zougman, A., Nagaraj, N. & Mann, M. Universal sample preparation method for proteome analysis. *Nat Methods* **6**, 359-362 (2009).
5. Cox, J. & Mann, M. MaxQuant enables high peptide identification rates, individualized p.p.b.-range mass accuracies and proteome-wide protein quantification. *Nature biotechnology* **26**, 1367-1372 (2008).
6. Cox, J. *et al.* Andromeda: a peptide search engine integrated into the MaxQuant environment. *Journal of proteome research* **10**, 1794-1805 (2011).
7. Yu, Z. *et al.* Optimizing 2D gas chromatography mass spectrometry for robust tissue, serum and urine metabolite profiling. *Talanta* **165**, 685-691 (2017).
8. Ingolia, N.T., Brar, G.A., Rouskin, S., McGeachy, A.M. & Weissman, J.S. Genome-wide annotation and quantitation of translation by ribosome profiling. *Curr Protoc Mol Biol* **Chapter 4**, Unit 4 18 (2013).
9. Ingolia, N.T. Genome-wide translational profiling by ribosome footprinting. *Methods in enzymology* **470**, 119-142 (2010).